A Literature Review on the Effects of Wind on the California Current System

Karen E. Norris
UCLA AOS 215
June 14, 2005

Introduction

The California Current System (CCS) along the west coast of the United States has been extensively studied. It is characterized as a perennial broad equatorward surface flow and a poleward undercurrent. There is also a seasonal poleward nearshore surface countercurrent. The basic circulation of the CCS has been well described, but the dynamics of the system are not completely understood, especially as to how they relate to the prevailing equatorward winds along the U. S. west coast.

This paper reviews the literature on the effects of wind on the CCS and synthesizes the results. Ocean and wind climatologies are described. Based on the climatologies, both coastal upwelling and offshore Ekman pumping appear responsible for the seasonal circulation pattern of the CCS. This is confirmed with analytical and numerical models.

Oceanographic and atmospheric data used in the reviewed studies varied in spatial and temporal resolutions. California Cooperative Ocean Fisheries Investigations (CalCOFI) hydrographic surveys have a spatial resolution of approximately 80 km and a temporal resolution of 3 months. CalCOFI data frequently are used as the ocean climatology in studies. Despite the poor temporal sampling, CalCOFI data are available from 1949, so there is statistical stability to the monthly means. Most of the papers reviewed used a CalCOFI ocean climatology. Unlike the ocean climatology, there is little consensus on the wind climatology. All researchers agree on the prevailing equatorward direction of the winds and the region of positive wind-stress curl near the coast, but the specific spatial structure of the wind field is still a matter of discussion. Wind fields used in the studies vary greatly in resolution and origin. Basin-wide, 2.5-degree resolution winds are the subject of one paper. Another paper uses very high-resolution wind estimates made from aircraft surveys in a 100 km square area. Other papers use modeled wind fields and not direct measurements. The structure of the wind field has a direct impact on the circulation pattern of the CCS. Thus, the use of different wind fields is a source of disagreement between the results of the reviewed studies.

The following section reviews the ocean climatology of the CCS. The next section discusses the effects of wind stress and wind-stress curl on ocean circulation. A section that describes the wind climatology of the United States West Coast follows. Results of the various studies are then discussed. The paper concludes with a summary.

Description of the California Current System

Many researchers have studied the CCS and all agree on a basic description of the circulation. The CCS is characterized by a broad equatorward flow, the California Current (CC), which is up to 1000 km wide off the western coast of the United States. There is a poleward undercurrent, the California Undercurrent. These flows are year-round. Then there is a seasonal (winter) poleward surface current immediately adjacent to the coast, beginning in the south near the SCB and extending north past San Francisco; this flow is often called the Davidson Current. In general, the CCS has weak eddying flow near the coast during the winter. The Davidson Current subsides in the spring and is overtaken by a surface equatorward jet. In the summer, this current becomes a strong coastal jet flowing at 20-30 cm/s. During the Coastal Ocean Dynamics Experiment (CODE), ADCP-measured speeds ranged up to 50 cm/s in the core of this inshore jet.

The CalCOFI has been collecting data in the CCS since 1949. Although the temporal resolution of this data is relatively poor (approximately every 3 months), the data have been collected consistently and thus comprise a very long-term time series. The spatial resolution is usually approximately 80 km although occasional special surveys are conducted with higher sampling.

Chelton (1982) used 30 years of CalCOFI data to compute the average steric height for the four seasons. Figure 1 shows the steric height of the sea surface relative to 500 db for the winter (January, left-hand plot) and summer (July, right-hand plot) seasons. Steric height contours can be used to infer relative velocity since the gradient of the steric height is proportional to the geostrophic flow. The offshore equatorward flow of the California Current can be seen in both plots. It approaches the shoreline in the summer months although there is some localized poleward circulation in the SCB. Bakun and Nelson (1991) noted that coastal bights along all eastern boundary currents were locations of persistent and cyclonic flow, consistent with the observation of enduring intense cyclonic wind-stress curl in coastal bights (discussed in a subsequent section). In the winter season, adjacent to the coastline, the Davidson Current appears as a strong poleward flow approximately 80 km wide and moving at 10 cm/s. The undercurrents are evident in Figure 2, which shows plots of the steric height of the 200-db surface relative to the 500-db surface.

Lynn et al. (2003) also used 30 years of CalCOFI data to determine the CCS climatology. They show the vertical profiles of geostrophic velocity for a survey line perpendicular to the coast at Point Reyes (north of San Francisco). Figure 3 shows the April and July long-term means. The number of observations for April ranged from 6 to 19 and for July from 6 to 16. There were fewer observations at the offshore stations. In April, the core of the surface equatorward California Current is nearly 400 km offshore and flows at a speed of 6 cm/s. There is a poleward undercurrent 200 km offshore that just broaches the surface. This flow is very slow and less than 100 km wide. There is a new equatorward jet adjacent to the shore. This current is over 100 km wide and moves at over 4 cm/s. By July, the equatorward flows have moved westward and have strengthened and joined to become one broad current. The entire surface current is equatorward. The current has one 10 cm/s section that is centered nearly 300 km offshore and a second section that is centered west of the CalCOFI sampling. The poleward undercurrent is nearshore and slow. These values agree with those by McCreary et al. (1987) and Chelton.

Another way of looking at the net flow is the accumulated volume transport. Lynn et al. computed the transport for 9 survey lines (spanning less than 2.5 degrees latitude) located north of Point Conception for March and April 1995. These values are representative of winter and spring seasonal mean values, respectively. Figure 4 shows these transport values as a function of distance from shore. In winter, there is a lot of variation among the surveys, with both poleward and equatorward transport. The net effect is a slight equatorward transport. However in spring, except for a few points nearshore, all of the transport is equatorward.

Sea temperature is another hydrographic parameter used to investigate the CCS. Lynn et al. plot the sea surface temperature (SST) for winter (March) and spring (April) 1995 in Figure 5. The winter isotherms tend to be perpendicular to the California shoreline with colder temperatures to the north and warmer to the south. In the spring, the

isotherms are parallel to the coastline, with the coldest temperatures closest to shore and warmer temperatures offshore.

Still another commonly measured hydrographic quantity is salinity. A southward-extending tongue of relatively low-salinity water marks the CCS during winter. The minimum salinity is typically found west of the velocity maximum. By spring, waters in the northern CCS are of even lower salinity than in winter. However along the coast there is higher salinity water. The salinity of this water is typical of water of more tropical origins. Figure 6 displays vertical sections of the spiciness for March and April surveys in 1995. Spiciness is a measure of temperature and salinity. Warm salty water is very spicy, whereas cool fresh water is not spicy. In the March cross-section, there is a subsurface anticyclonic eddy, centered at approximately 122^{o}W and at depths of 100 to 400 m (more easily seen in the cross-section of geostrophic velocity, not shown). This eddy is composed of warm salty water, indicating its source as the California Undercurrent. In April, there is a shallow (<150 m) surface equatorward nearshore jet. This jet is less spicy than the water that was there in March. The source of this flow is northern, cool, fresh water. The April California Undercurrent, occupying nearshore water in depths of 100 to 500 m, has now become stronger and spicier.

In summary, the CCS is characterized by a cool, less-saline perennial equatorward surface flow that typically is centered several hundred kilometers offshore and is several hundred kilometers wide. The California Undercurrent is a spicy poleward flow. The Davidson Current is a seasonal, relatively spicy, poleward, nearshore surface flow in the winter. Finally, there is a strong nearshore surface equatorward jet in the summer months that has cool temperatures. Beneath this jet the California Undercurrent becomes stronger and spicier, flowing in the poleward direction.

Wind Effects

Two processes thought to influence the CCS circulation are coastal upwelling caused by Ekman divergence at the coastline and Ekman pumping produced by Ekman divergence and convergence offshore.

Coastal upwelling is a result of offshore movement of water in response to wind stress. The surface wind stress causes a net horizontal movement of water offshore. Deeper water upwells to replace the water that has moved offshore. In so doing, the isopycnals (isotherms) rise towards the coast. The sea surface drops in response to the colder, denser waters that are closer to the surface. Since the sea surface slopes down towards the coast, a geostrophically-balanced equatorward flow develops (assuming an equatorward wind). Upwelling brings nutrient rich water to the surface. As a result, there will be high primary production in the area of upwelling. Associated with this is an abundance of zooplankton. Thus, a typical signature of coastally-upwelled water is colder SST and a depressed sea surface height (SSH) adjacent to the shore. There will also be higher zooplankton distributions than elsewhere.

Ekman pumping is a response to a spatially variable wind field. The curl of the wind stress results in the divergence (or convergence) of surface Ekman transport. To conserve mass, a vertical velocity results. The vertical velocity is expressed as

$$w = \hat{k} \cdot \left(\vec{\nabla} \times \frac{\vec{\tau}}{f \rho} \right).$$

A positive wind-stress curl results in an upward velocity, i.e., an upwelling of water. Conversely, negative wind-stress curl produces downwelling of surface water. Sverdrup determined the steady-state response to wind-stress curl as

$$\int_{-\infty}^{0} v\mathrm{d}z = \frac{1}{\rho\beta}\left(\frac{\partial\tau_y}{\partial x} - \frac{\partial\tau_x}{\partial y}\right).$$

Since the latitudinal variation of the Coriolis parameter, β, is df/dy, a positive wind-stress curl results in a poleward vertically-integrated Sverdrup transport. This poleward transport is irrespective of the direction of the wind stress as long as there is positive wind-stress curl. Another effect of the latitudinal variation of the Coriolis force is the generation of westward propagating Rossby waves. These ultimately will bring the ocean into steady-state Sverdrup balance. The phase speed of the Rossby waves is less than 10 cm/sec. Therefore, a minimum time scale of 2-3 months is required for steady-state equilibrium.

To achieve a nearshore poleward geostrophic flow, the slope of the sea surface must slope down, away from the coast. If there is an equatorward flow further offshore, then there will be a depression, a trough, in the sea surface between the two opposing flows. To compensate, the thermocline will dome upward towards the depression. Figure 7 from Chelton depicts a diagram of the sea surface and thermocline configuration in these circumstances. The hydrographic signature of Ekman upwelling is a depression in the SSH and doming of the isopycnals. Again, there may be an increased abundance of zooplankton in association with the upwelled nutrient-rich water.

Conversely, if the wind stress is poleward or the wind-stress curl is negative then downwelling results. The signature of downwelling is a depression of the thermocline and a raised sea-surface height.

The question with respect to the CCS and other eastern boundary currents is what is the combined effect of wind stress and wind-stress curl on the circulation. McCreary et al. used analytical and numerical viscid models to answer that question. They used linearized equations of motion with a stably-stratified background density state and associated Väisälä frequency. They assumed alongshore geostrophy so that the thermal wind relation held everywhere. Also, they used conditions of no-slip at the coastline and finite-slip at the offshore boundary. Parameters that varied were the density (linear or with a strong, near-surface pycnocline), the horizontal and vertical mixing coefficients, the bottom depth, the southern boundary for the wind field, and the wind field itself. The analytical model used a flat bottom and the numerical model included a continental shelf. They compared solutions to the model forced by wind stress, positive wind-stress curl, and by a combination of wind stress and positive wind-stress curl. The wind was both steady and periodic.

They modeled the climatologic wind field off the California coast with an idealized wind. The equatorward wind peaked in magnitude 200 km off the coast and tapered to zero wind stress at the coastline. This gives a positive wind-stress curl out to 200 km, with the maximum curl at the coast. The latitudinal extent of the wind field varied. The northern extent of the wind field was fixed at 40 degrees (Cape Mendocino) and the southern limit was either 20 degrees or 30 degrees (southern Baja California and

Ensenada, respectively). The wind stress was constant in the center of the latitudinal extent, tapering to zero within the end 2.5 degrees.

Figure 8 shows zonal sections of the analytical model solution for the region of ocean just north of Point Conception for the four seasons. The model used the combination of periodic wind stress and positive wind-stress curl, a strong near-surface pycnocline, and remote winds. The bottom depth was 1000 m, although the parametric study showed that the depth had little impact on the solutions. The June solution shows the case when the wind-stress forcing dominates over the wind-stress curl effects. The surface flow is entirely equatorward, with two jets. The inshore equatorward jet is much stronger than the offshore flow. There is a broad poleward subsurface countercurrent. By September, when the wind stress has weakened, the coastal jet has correspondingly weakened and diminished. The surface flow is still entirely equatorward. In December, the wind stress is very weak and the forcing by positive wind-stress curl dominates. There is a very strong poleward nearshore surface flow. A subsurface equatorward countercurrent balances this flow. Offshore, there is still an equatorward flow. When spring comes in March, the wind stress strengthens and a strong inshore equatorward jet appears. The surface nearshore poleward flow weakens and becomes smaller, bordered offshore by the perennial equatorward flow and inshore by the seasonal equatorward jet. There is a broad poleward subsurface countercurrent with a small, distinct jet below the new surface coastal flow. In summary, when the wind stress is strong, there is surface equatorward flow inshore and offshore balanced by a subsurface poleward flow. When the positive wind-stress curl dominates the forcing, there is a poleward inshore flow and equatorward offshore flow. Below, there are opposing countercurrents.

The effects of a continental shelf are shown in Figure 9. These results come from the numerical model. Two months are shown, June and December, when the wind stress and positive wind-stress curl dominates the forcing, respectively. The results are very similar to the analytical model results with a flat bottom. However, the presence of a shallow shelf strengthens the coastal jet and weakens the undercurrent.

McCreary et al. concluded that generation of a nearshore poleward surface flow is possible with positive wind-stress curl. Offshore equatorward flow is also generated, but only as a result of vertical mixing. The forcing from the alongshore winds is responsible for the inshore equatorward jet. Both the steep pycnocline and the variation in the Coriolis force broaden the inshore flow while the remote wind forcing from the south strengthens the flow. The inshore equatorward jet is strong enough so that the net effect in summer is to reverse the poleward flow resulting from the wind-stress curl.

Enriquez and Friehe (1995) also used analytical and numerical models to determine the effect that wind stress and wind-stress curl would have on the circulation. They started with linearized, reduced-gravity equations of motion. They used a two-layer model in which the lower layer is dynamically inactive and the upper-layer's motion is represented by the first baroclinic mode. There is no slip at the coast and slip at the offshore boundary. The idealized wind field produces a cross-shore curl profile that is positive and peaks 15 km from the shore. The curl decreases to zero far offshore. Steady and periodic winds produced similar results. Figure 10 shows the solutions to the analytical model. In the left-hand plot, the upwelling rate forced by wind stress is compared to the upwelling rate due to wind stress and wind-stress curl. The combination of stress and curl more than doubles the rate of upwelling due to just wind stress. The

difference between these two upwelling rates is plotted in the right-hand plot as the solid line. The dashed line represents the difference in upwelling rates when the maximum curl value is far offshore. The offshore curl dramatically increases the upwelling rate. An additional 4 m/day are upwelled in the 20 km offshore due to nearshore curl and an additional 10 m/day are upwelled due to far-offshore curl. This shows that the location of maximum curl greatly affects inshore upwelling. Also, the area of the curl is important since the application of a localized positive wind-stress curl results in an increase in upwelling over a larger area than the horizontal extent of the curl itself.

The upwelling process has thus far been examined with only simple models. Capet et al. (2004) used a complex model for the Southern California Bight (SCB) and Central California Coast, and an atmospheric model to examine the effect the wind has on upwelling. They showed that the Regional Ocean Modeling System (ROMS) could produce reasonable SSTs for the SCB, given a reasonable representation of the wind field.

To look at the effect that wind has on the upwelling, ROMS was forced with two different wind fields. The first field, "BLD", is a blend of the Coupled Ocean/Atmosphere Mesoscale Prediction System (COAMPS) winds at 9-km horizontal resolution and QuikSCAT ("QCT") scatterometer analyses. QCT winds are the second wind field. Scatterometer winds are unreliable within 50 km of the shore, so the nearshore profile of BLD is that of the COAMPS wind field. The 9-km COAMPS wind has an offshore peak in wind stress at 60 km with the wind stress decreasing until a minimum at 24 km offshore. The wind stress rapidly increases to a maximum value at the shore. This profile differs from those measured by Enriquez and Friehe and by Münchow (2000), discussed in the following section. Their wind measurements, at a much higher resolution than the COAMPS winds, showed an offshore profile for equatorward winds consisting of a peak in wind stress far offshore (>100 km), decreasing towards the coast with a minimum in wind stress at the coast. Another problem with the COAMPS winds is that the three available resolutions, 3 km, 9 km, and 27 km, are not even smoothed versions of one another. The 3-km winds have a minimum stress at 9 km offshore, the 9-km winds have the minimum 24 km offshore, and the 27-km winds have only a slight local minimum 55 km offshore. Which resolution wind is most representative of the actual wind field is not clear. The nearshore wind profile is critical to determining the relative importance of Ekman pumping to coastal upwelling. So Capet's second wind field, QCT, is especially inadequate for nearshore upwelling studies.

Nevertheless, Capet used the two wind fields to look at nearshore upwelling. Since ROMS incorporates more accurate assumptions and circulation dynamics, including eddies, the results may be more indicative of the upwelling process. Figure 11 compares the wind stress and wind-stress curl of the two wind fields. BLD has maximum positive wind-stress curl immediately adjacent to the coast. QCT has two areas of maximum positive wind-stress curl, of much lower magnitude than that of BLD. These areas are well offshore.

Both wind fields forced model solutions that look realistic for the CCS, however there were discrepancies with both solutions such that one cannot be declared a better "match" to the ocean climatology. Based on the discussion of the upwelling process, the BLD solution should produce results that show a combination of coastal and Ekman upwelling since the curl has a high positive value and it is close to shore. The QCT

solution should be representative of solely coastal upwelling since the curl is small and well offshore. Figure 12 shows vertical cross-sections of the temperature profile for the two solutions. Indeed, the BLD temperature profile shows doming of the isotherms in addition to a rise in isotherms at the coast. The doming occurs in the same location as the maximum curl. This profile is what is expected of Ekman and coastal upwelling. The QCT temperature cross-section shows only a sharp rise in isotherms at the coast, indicative of just coastal upwelling.

Capet et al. also plotted the alongshore velocity profiles for the two solutions, as shown in Figure 13. The BLD solution has a shallow equatorward surface flow which peaks at 4 cm/s. Just offshore, there is a poleward surface flow as the undercurrent reaches all the way to the surface. The poleward undercurrent flows at a maximum speed of over 12 cm/s. Immediately next to the coast is a very narrow and slow equatorward flow. The QCT alongshore flow varies greatly from the BLD flow. The equatorward flow is inshore and has a width of approximately 40 km, with an area of virtually no flow where the very slow undercurrent broaches the surface. The QCT equatorward jet is well defined and flows at nearly 6 cm/s. The QCT poleward undercurrent is much narrower, deeper, and slower than the BLD undercurrent. These solutions contrast with McCreary et al.'s model results. McCreary et al. found a weaker, broader, and deeper undercurrent than those determined by Capet et al. Also, the McCreary et al. surface equatorward current flowed deeper and faster (>18 cm/s) than the Capet solutions. As described in the section on CCS climatology, the mean summer circulation consists of a broad equatorward surface flow with speeds of 20-30 cm/s. There is no surface poleward flow except for within the SCB. Perhaps the discrepancy between the model solutions is due to the difference in the forcing wind fields.

In response to Enriquez and Friehe's study on the effect of Ekman pumping on upwelling rates by coastal Ekman divergence, Capet et al. calculated Lagrangian diagnostics for the two model solutions. Parcels were released from two depths above 100 m and then followed. This provides a measure of the upwelling of nutrients. With deep upwelling, the BLD solution was more evenly distributed, with even amounts of upwelling occurring offshore as with nearshore. Most of the deep upwelling in the QCT solution was nearshore. For both QCT and BLD solutions, approximately 40% of the total number of upwelled parcels occurred within 10 km of the coast at all depths. So even for the BLD-forced model solution, which used a combination of wind stress and positive wind-stress curl, the upwelling due to coastal divergence was greater than the offshore Ekman upwelling. No matter which two depths were used to quantify the upwelling, the QCT-forced model results had greater upwelling. This contrasts with the results of Enriquez and Friehe that suggested that the addition of offshore Ekman upwelling results in a net upwelling rate equal to double that due to coastal divergence by itself. However, there were differences in the relative strengths of the wind stress and wind-stress curl and the cross-shore profile of the wind. Enriquez and Friehe used a maximum wind stress of 0.1 Nm^{-2} (1 Nm^{-2} = 1 Pa = 0.1 dyn cm^{-2}) whereas Capet et al. used a higher value of 0.146 Nm^{-2}. The curl values differed greatly between the two studies. So again, the differences in the results may be due to the very different wind fields. This illustrates the importance of the wind field to the upwelling process.

To summarize the effects of wind on upwelling and flow, in the presence of alongshore wind stress and positive wind-stress curl the circulation of the CCS should

include a perennial offshore equatorward flow and a subsurface poleward countercurrent. There will be a seasonal inshore poleward current when the alongshore wind-stress is weak and the wind-stress curl is very positive (winter months) and a seasonal inshore equatorward current when the alongshore wind-stress is equatorward and very strong (spring and summer). Upwelling from equatorward, nearshore winds will be enhanced by the perennial positive wind-stress curl offshore. Of great importance is the cross-shore profile of wind stress and the locations of the positive wind-stress curl and the contour of zero wind-stress curl since these determine the relative strengths of the coastal upwelling and Ekman pumping contributions to the ocean circulation.

United States West Coast Wind Climatology

There is some consensus on the general patterns of wind off the west coast of the United States. However, there is disagreement on the specifics, such as the location of contours of zero wind-stress curl and wind stress local maximums and minimums. Much of the disagreement is related to the lack of adequately-resolved measured wind fields.

The National Centers for Environmental Prediction (NCEP) coarsely-resolved wind reanalysis is the accepted wind pattern. Murphree et al. (2003) describe the patterns in Figure 14, which shows the 2.5-degree resolution NCEP wind vectors for the North Eastern Pacific (NEP) basin for the months of January and July based on data collected from 1968-1996. The vectors are overlaid on the wind-stress curl. Positive curl is colored blue, negative curl is red. Winter winds in the NEP have a large anticyclonic circulation representing flow about the North Pacific High (NPH). To the northwest, over the northern part of the NEP is a large cyclonic circulation around the Aleutian Low (AL). Anticyclonic flow is dominated by negative wind-stress curl and cyclonic flow by positive wind-stress curl. There is a narrow strip of positive wind-stress curl along the coast of California. This region of positive curl is associated with the onshore weakening and the cyclonic turning of the coastal winds on the eastern flank of the NPH. Likewise, there is a strip of negative curl along the coast north of California, extending to southern Alaska. This strip is associated with the onshore weakening and anticyclonic turning of winds on the eastern flank of the AL.

The summer pattern of wind is very similar, however there is no negative wind-stress curl near the Alaskan coast. The large region of negative wind-stress curl due to the NPH is stronger and centered further to the northwest (closer to the coast of California). In addition to the movement of the NPH, there is a thermal low over the southwestern portion of the United States. The western flank of that low provides additional strong equatorward winds to those from the NPH eastern flank. So the coastal strip of positive wind-stress curl is stronger and extends further north. Murphree asserts that the maximum wind-stress curl along the west coast is during the months of May through July. This agrees with other studies. Figure 15 from Chelton shows the seasonal cycle of wind stress and wind-stress curl based on winds from the Fleet Numerical Oceanography Center (FNOC) with a 300-km resolution. Chelton placed the wind-stress curl zero-contour line roughly parallel to the coastline and approximately 200-400 km offshore. Positive wind-stress curl is shoreward of the line, negative curl seaward. He asserted that the curl magnitude is maximum immediately adjacent to the coast.

Throughout the year the strongest winds occur on the flanks of the NPH and the AL. In those regions there is large shear-vorticity and wind-stress curl values. In addition

to the influence of strong flank winds, the CCS is subject to winds that undergo topographic forcing. The California coast has steep mountains that parallel the coastline. This topographic feature constrains the winds.

The resolution of the NCEP wind maps is too coarse to determine the distance offshore of the wind-stress curl zero-contour line. Bakun and Nelson use historical shipboard wind estimates from 1950-1979 to determine 1-degree resolution wind stress and wind-stress curl maps for 6 2-month periods. In the SCB, the density of observations in a 1-degree quadrangle ranged from 5,000-20,000. Their maps show a maximum positive wind-stress curl in the SCB year-round with the exception of August and September. In those months the maximum curl is off Cape Mendocino in northern California. Figure 16 shows the wind stress and wind-stress curl maps for June-July and December-January time periods.

Bakun and Nelson place the zero contour line of wind-stress curl 200-300 km off shore where the maximum of alongshore wind stress is located. The wind stress decays towards the coast, defining a region of positive wind-stress curl. This is true year-round along the coast of California. However, to the south, the maximum wind stress occurs at the coastline at Punta Baja in Baja California. So negative wind-stress curl exists along parts of Baja California. In the Pacific Northwest, there is a variable mixture of both cyclonic and anticyclonic winds, probably associated with winter and spring storms. That region sees periods of negative wind-stress curl immediately adjacent to the coast. The maximum equatorward wind stress is located approximately 10 km off the coast.

Bakun and Nelson also noted the effects of topographic forcing. Regions near capes experience particularly intense cyclonic (positive) wind-stress curl. In addition to that additional forcing, they report from an independent reference that the low-level winds during summer months may be strengthened by thermal forcing from the land-ocean temperature contrast.

Enriquez and Friehe conducted a much higher spatial-resolution study using wind measurements by the National Center for Atmospheric Research (NCAR) to estimate the wind field near Point Arena in northern California. In the 1989 Shelf Mixed Layer Experiment (SMILE), an aircraft flew multiple cross-shelf, low-level (30 m) tracks in a 100-km square area. Sampling in the along-track direction was 3.5 m and the tracks were spaced 15 km apart. In the months of February and March a total of 23 flights were flown, catching periods of downcoast and upcoast winds.

Enriquez and Friehe note that the coastal mountain ranges cause rectification of strong winds so that the winds tend to be either downcoast or upcoast. The profile of the winds depended on the orientation. Downcoast winds are strongest offshore while upcoast winds are strongest nearshore. For downcoast winds, the speed of the wind varied in the cross-shore direction and for upcoast winds the speed varied in the alongshore direction.

Enriquez and Friehe also looked at wind estimates from the 1982 CODE taken in the same area as SMILE. CODE was conducted over a smaller area but with similar high-resolution measurements. Very similar values of wind stress and wind-stress curl were obtained from the two experiments. They were able to measure the average stress and curl values for the two conditions in SMILE. Downcoast wind stress ranged between 0.07 to 0.57 Pa and upcoast wind stress ranged between 0.05 to 0.23 Pa. In CODE, wind stress values exceeded 0.5 Pa. Previous estimates for the downcoast-wind stress for the same

geographical area are 0.031 for February and 0.089 Pa for March. These low estimates may be a result of averaging over a monthly time period when winds are variable, especially during winter months. Also, the previous estimates are based on shipboard estimates of wind, which have poor spatial resolution and probably do not accurately sample the wind field.

During both experiments, wind-stress curl was predominantly positive, regardless of the wind direction. Figure 17 shows the wind-stress curl for a day of downcoast winds and a day of upcoast winds. Negative curl is colored blue. Maximum positive curl is colored red. Over all the flights, for downcoast winds the maximum curl value exceeded 1.5 Pa/100 km and the minimum value was –0.4 Pa/100 km. For upcoast winds, the maximum curl value was 1.0 Pa/100 km. There was a persistent local maximum near Point Arena, again, regardless of the wind direction. This local maximum ranged from less than 0.2 Pa/100 km during weak winds to over 1.5 Pa/100 km during strong winds. The local maximum was positioned 5-20 km offshore with no systematic dependence on the wind direction.

Münchow (2000) conducted an experiment similar to SMILE in southern California near Point Conception. In April and May of 1983, 20 aircraft flights collected wind and atmospheric data. The wind measurements were interpolated onto a grid with longitudinal resolution of 5.7 km and latitudinal resolution of 3.7 km. During the month of flights, the winds were variable. The result is that the mean stress value of 0.09 Pa is low compared to daily values. On a day of strong downcoast winds, the mean wind stress was 0.31 Pa. On a day of upcoast winds, the mean wind stress was 0.26 Pa. These values are very similar to those in the SMILE and CODE experiments.

Although Münchow does not compute the curl values, instead computing the upwelling rates (positive indicates upwelling and positive curl), his results were qualitatively similar to Enriquez and Friehe's. No matter the wind direction, the resulting wind-stress curl was positive. This is true especially to the south of Point Conception. Münchow computed upwelling rates for each of the collections. On the day of strongest downcoast winds, the Ekman upwelling velocity is 20 m/day. On the day of strongest upcoast winds, the Ekman upwelling velocity is 4 m/day in an area of 10 km by 80 km. Further south of that region there was downwelling. Münchow placed the line of zero stress approximately 10 km offshore of Point Conception. He stated that the area of maximum curl was closer to the shore. This is similar to the findings of Enriquez and Friehe.

Perhaps the most interesting part of Münchow's experiment was the inclusion of atmospheric profiles. Rawinsonde data were collected at Vandenberg Air Force Base, just north of Point Conception. From these data he estimated the buoyancy frequency N, which is a measure of the vertical stability. The stability maximum occurs during a temperature inversion with warm dry air aloft and cooler moist air below. Figure 18 shows the records of surface winds and SST at a National Oceanic and Atmospheric Administration (NOAA) buoy near Point Conception and the buoyancy frequency for the lower atmosphere at Vandenberg AFB. Notice that the persistent equatorward winds (upwelling-favorable) after May 6 were accompanied by lower SSTs and increased atmospheric stability. The atmospheric stability allows persistent equatorward winds, and the upwelling caused by those winds lower the SST, which cools the low-level air, which in turn enhances the atmospheric stability. Also, the cooler water temperatures reduce the

frictional drag at the air-sea interface, which will increase the surface winds. This suggests that there is a positive feedback between the atmospheric stability, the surface winds, and the ocean upwelling. Enriquez and Friehe also observed strong downcoast low-level winds below stable atmospheric inversions during the summer.

In summary, the winds off the United States west coast are characterized by prevailing equatorward winds. These winds strengthen in the summer months from the positions of the NPH and the thermal low-pressure system in the southwestern US. During winter months, the wind direction is more variable so that upcoast (poleward) winds are present in addition to the downcoast (equatorward) winds. The winds experience topographic forcing due to the coastal mountain ranges and the many capes and headlands. No matter the wind direction, there is persistent positive wind-stress curl adjacent to the coast. The positive curl is perennial in southern California and seasonal (in the spring and summer) in northern California. The highest resolution wind estimates place the maximum curl 5-20 km offshore, with the wind stress approaching zero either at the shore or just offshore. The maximum wind-stress curl occurs in the spring and summer months.

Discussion

In general, the reviewed analyses are a comparison of observations to expectations based on theory and models. The complexity of the models varies from simple to complicated. If the model output resembles the observations, then one might conclude that the model assumptions are correct.

There is little disagreement that the alongshore wind stress plays an important role in the circulation of the CCS. From theory and simple models, the expectation is to have depressed SSHs and colder SSTs when the alongshore wind stress is equatorward. Lynn et al. compared time series of the upwelling index, a measure of the strength of equatorward wind stress, to the adjusted sea level at Monterey. Figure 19 shows the two time series. A positive index indicates equatorward wind stress. In the beginning of March, there is a period of very negative upwelling indices. Correspondingly, there is a period of dramatically raised sea level, a sign of downwelling. The month of April is marked by a series of strongly positive upwelling-indexed periods. This time period shows a steadily decreasing SSH, with the lowest surface immediately following the highest upwelling index. Qualitatively this is the expected behavior for wind stress and resultant coastal upwelling and downwelling.

Two fairly-high resolution CTD surveys were conducted during the time of the upwelling-index record. The times of these surveys are denoted on Figure 19 with gray lines. The March survey, which had values near the winter climatological mean, occurred when there were variable winds. The April survey took place during multiple upwelling periods. Figure 5 shows the SST for the two surveys. The April SST plot clearly shows a narrow band of very cold temperatures near the shore. This is a sign of coastal upwelling. This figure, combined with the April profile of spiciness in Figure 6, reveals a narrow coastal equatorward jet, a strong and narrow undercurrent, and a broad offshore equatorward flow. This agrees somewhat with McCreary et al.'s simple model predictions. However, observations show only a narrow undercurrent close to shore, but the model predicts a broad undercurrent with a narrow jet close to shore. McCreary et al.

did not discuss how the various assumptions and parameter choice affect the undercurrent's dimensions.

Chelton's investigation of the CCS centered on zooplankton abundance. Figure 20 shows his plots of average zooplankton displacement volume (left-hand plot) and the average longshore geostrophic transport in the upper 500 m, which includes the California Undercurrent. As mentioned earlier, maximums of zooplankton abundance are generally associated with upwelling of cold, nutrient-rich water. Chelton noted that if coastal upwelling was the sole mechanism for nutrient-rich water to arrive at the surface, then the corresponding zooplankton maximum should occur next to shore with the abundance decreasing with distance from the shore. This is only true off Baja California. North of Baja California, the zooplankton abundance peaks well offshore. Chelton does note that there are local maximums close to the California coast that the CalCOFI surveys do not sample. These maximums are indicative of coastal upwelling. The offshore zooplankton maximums occur at the location of maximum horizontal shear in the longshore transport. Nearshore transport is poleward and offshore transport is equatorward. The flow in the region of the zooplankton maximum is very weak, providing a stable environment with little dispersal of the nutrients. The offshore maximums of zooplankton abundance indicate that there is another mechanism bringing nutrient-rich water to the surface, not just coastal upwelling.

In addition to offshore cold, nutrient-rich water (zooplankton abundance), another sign of Ekman upwelling is the doming of the isopycnals. Figure 21 shows the average July temperature profiles for Point Conception and San Diego. At both locations, the isopycnals tilt upwards very close to shore, indicative of coastal upwelling. However, 100 km offshore the isopycnals form domes, a clear sign of Ekman upwelling. Not shown are the measured nutrient concentrations along the CalCOFI line off Point Conception. The vertical profile of nitrate shows very clear doming and upwelling of nitrate 100-200 km offshore. Satellite chlorophyll images show that there are areas of high chlorophyll approximately 100-150 km offshore. The doming of the isotherms and nitrate occurs at approximately the same location as the depression in steric height (Figure 1), the reversal of transport direction, the maximum positive wind-stress curl, and the maximum abundance of zooplankton. These correspondences are evidence for Ekman upwelling and not coastal upwelling. Chelton finds what Bakun and Nelson noted, that coastal upwelling influences the circulation nearshore and Ekman pumping affects the offshore circulation.

Münchow had excellent high-resolution measurements of the wind field off Point Conception in 1983. Unfortunately he didn't have concurrent hydrographic data during the expected periods of strong upwelling (April). CTD data were available from the spring of 1984, but only wind estimates from a buoy were available. The survey was conducted in the center of a period of intense upwelling-favorable winds that exceeded 10 m/s for nearly 20 days. Measured 30-m currents in the area varied from 10 to 80 cm/s in the poleward direction. Figure 22 shows the depth of the 26.5 isopycnal surface south of Point Conception. Against the northern shore, the isopycnal is approximately 100 m deep. At the southern shore of the Santa Barbara Channel (near the Channel Islands), it is 80 m deep. In the center of the channel though, the isopycnal approaches a depth of 60 m. This doming of the isopycnals is clear in a vertical profile of the channel, shown in Figure 23. A comparison of the density surface in Figure 22 with the computed Ekman

pumping velocity based on the previous year's high-resolution wind measurements shows similarity in the location of the positive wind-stress curl. This comparison is shown in Figure 24. The plots have been cropped and rescaled to be the same size. As with Chelton's results, the doming of the isopycnals is indicative of Ekman upwelling and not of coastal upwelling.

Thus far the reviewed studies have compared hydrographic measurements to predictions based on actual wind fields or to simple models forced with idealized wind fields. Di Lorenzo (2003) studied the wind effects on the CCS, mainly the southern portion, in a manner akin to Capet et al. He forced ROMS with three wind fields and compared the results to a CalCOFI climatology. The differences between the results highlight the effects of wind stress with and without wind-stress curl on the circulation. One solution had high correlations with the climatology. This solution exposes the Rossby wave dynamics that the simple models did not.

Di Lorenzo used three wind fields with different resolutions and cross-shore profiles. The first wind field is from a regional atmospheric model, the Regional Spectral Model (RSM), which is derived from the NCEP reanalysis. The RSM winds have a horizontal resolution of 50-25 km; daily values were averaged to form monthly means. The second wind field is from the Comprehensive Ocean-Atmosphere Data Set (COADS) and has a horizontal resolution of 2 degrees. These data are available as monthly means. The final wind field is the NCEP 1 x 1.5 degree resolution of monthly means. Figure 25 compares the wind-stress curl of the three wind fields. The curl of the RSM winds best matches the curl shown by previous researchers although the region of maximum curl is further offshore and the magnitude is smaller than the observed curl.

Figure 26 shows results of the model, as forced by the three wind fields. The annual mean depth of the 26.5 isopycnal is plotted. This isopycnal represents the interfacial depth of the first baroclinic mode. The left-hand panel shows the CalCOFI climatological mean based on 50 years of collections. The offshore broad equatorward flow of the CC is readily apparent, as is the inshore poleward flow in the SCB. From left to right, next to the climatology, are the surfaces for the RSM, COADS, and NCEP winds. All of the wind-forced model results capture the offshore equatorward CC. However, only the RSM results have the inshore recirculation in the SCB. The NCEP results do show some recirculation, but it is far offshore. The area of recirculation is collocated with the maximum positive wind-stress curl. Correlations between the climatology and the model results quantify the comparisons. The RSM winds had a correlation of 91% for the depth of the isopycnal. COADS and NCEP correlations were 85% and 79%. A better measure of model performance is the correlation of the zonal gradient, dh/dx, which is a proxy for geostrophic flow. Again, RSM had the highest correlation, 48%. The correlations for COADS and NCEP were very low, -15% and 5%, respectively. Not surprisingly, the better the resolution winds and representation of the wind-stress curl, the better the results. With the RSM winds, the leading-order dynamics of the CCS are represented in the model results.

One feature that Di Lorenzo explored in depth is the westward propagation of the spring-summer equatorward jet and associated hydrographic anomalies that have been noted by Lynn et al., Chelton, and others. The latitudinal variation of the Coriolis force generates westward propagating Rossby waves, bringing the ocean into steady-state Sverdrup balance in response to wind-stress curl. In spring, the nearshore thermocline

raises in response to alongshore winds and wind-stress curl. This shoaling moves offshore as spring and summer progress. This westward movement can be seen in the CalCOFI climatology. The shoaling occurs over the entire continental shelf. Figure 27 plots the 26.5 isopycnal depth anomaly of a particular transect across the SCB as a function of time and offshore distance for the CalCOFI climatology and the three model solutions. This comparison highlights the importance of both wind stress and wind-stress curl to a realistic solution. The upper left-hand plot shows the westward propagation of a depth anomaly in the CalCOFI climatology. The anomaly develops across the entire continental shelf in early spring and deepens as summer progresses. Beginning in June, the anomaly moves westward so that by September and October the isopycnal depth anomaly is then located in the deep ocean, 300 km offshore. By March of the following year, the anomaly has translated to a location at least 500 km offshore. The RSM westward propagation pattern, seen in the second plot in Figure 27, correlates well with the observed CalCOFI pattern, with a coefficient of 0.73. The propagation pattern corresponds to the development of the wind-stress curl: the positive wind-stress curl increases in strength in spring through the summer into a region of intense curl over the entire shelf region. The COADS and NCEP patterns have low correlation with the observed propagation pattern, -13% and 31%, respectively. The COADS result shows the westward propagation, but the anomaly develops initially only nearshore. The COADS winds had minimal curl. The NCEP result shows the anomaly shoaling over the shelf, but later in the year and only after a nearshore anomaly has propagated offshore. The NCEP winds do have curl, but further offshore and much weaker than the RSM wind. The positive curl is essential to the development of the anomaly over the entire shelf and the alongshore wind stress is a critical ingredient to the westward propagation.

Lynn et al. were able to track the westward propagation of several eddies with spiciness and flow patterns. A particular eddy that was located off Point Conception in March had moved offshore by April. Additionally, using data from an independent source, they noted that the SSH gradients and the eddy kinetic energy reached maximum values in the summer to fall time-frame. These quantities also showed an offshore seasonal progression. Lynn et al. concluded that the westward propagation was indicative of Rossby wave dynamics.

Di Lorenzo investigated the Rossby wave dynamics further. He linearized a Primitive Equation model about a state of rest, forced it with the RSM winds, and dropped the advection term since he was interested only in the quasi-linear long-wave response of the system. He integrated the model for 12 years, which was insufficient time for the development of eddies. The coastal upwelling is not resolved in this model, so only the effects of the wind-stress curl appear in the solution. Figure 28 shows the SSH anomaly as a function of time and distance from shore for the linearized model forced by RSM winds. The anomaly is negative, i.e. the sea surface is depressed, associated with Ekman upwelling. The first plot, (a), shows the outer-shelf development of a SSH anomaly in May and its subsequent westward propagation for the model which includes a latitudinal variation of the Coriolis force. This pattern correlates 80% with the non-linear ROMS solution. Di Lorenzo also ran the model with β equal to zero. This solution is depicted in the second plot, (b), of Figure 28. Here there is a seasonal development of the SSH anomaly but no westward propagation. These results confirm the earlier observation

that the Ekman upwelling is responsible for the development of the SSH anomaly across the shelf width and at least initiates the subsequent westward propagation.

The table in Figure 28 reports the correlation coefficients for different cross-shore sections between the non-linear ROMS solution and linear model with a non-zero β. Inshore where the positive curl is greatest, there is a 75% correlation. The correlation drops and then increases to 85% far offshore, indicating that other, non-linear, processes are important in the region where the correlation decreases. In satellite observations of SSH and SST, there are mesoscale features such as cold filaments and mushroom-shaped patterns that are associated with strong eddy fields in this same region. It appears then that the Rossby wave dynamics cause dynamical instabilities that generate eddies and meanders in this region over the continental slope.

Observational analyses have shown excellent qualitative agreement between expectations from simple models and hydrographic measurements. A complex eddy-resolving model is able to duplicate the observations and quantify the effects of the alongshore wind stress and the wind-stress curl on ocean dynamics. The alongshore equatorward wind stress affects the nearshore ocean circulation. The ocean responds to wind-stress forced coastal upwelling with depressed sea surface heights, colder sea surface temperatures, upward tilted isotherms and isopycnals, and a coastal equatorward surface jet. Offshore Ekman upwelling forced by positive wind-stress curl appears in the hydrography as a depression or trough of depressed sea surface height and temperature in an area greater than that of the positive curl. Also associated with this is an abundance of zooplankton and nutrients at the surface. Beneath the surface, the isotherms, isopycnals, and isolines of nutrients form domes. The positive wind-stress curl creates an offshore equatorward surface current and an inshore poleward flow. Together, the wind stress and wind-stress curl cause an ocean anomaly in temperature and density across the continental shelf in the spring. Through Rossby wave dynamics, this anomaly propagates westward offshore to deeper water. The westward propagation suffers instabilities which spawn meanders and eddies.

The greatest defect of the reviewed studies is the inaccuracy of the wind field used to predict the behavior dynamics. Certainly concurrent large-scale high-resolution CTD and atmospheric surveys will answer more questions about the California Current System dynamics. A more affordable approach to answering these questions is a fully parametric study with either a simple model or an eddy-resolving model. It is the combination of wind stress and wind-stress curl that controls the California Current System. The forcing wind-field should be parameterized to reflect the different possible configurations, instead of using a single idealized wind field.

Summary

Theory and simple models predict the effects of wind stress and wind-stress curl on eastern boundary currents. By itself, alongshore wind stress creates coastal up- (or down-) welling. Coastal upwelling has a hydrographic signature of depressed sea surface heights, lowered sea surface temperatures, higher abundances of nutrients and zooplankton, tilted isolines of the same quantities, and an equatorward surface inshore current that has a corresponding poleward undercurrent. Wind-stress curl induces offshore Ekman pumping. Positive curl results in upwelling, while negative curl results in downwelling. Ekman upwelling is marked by a depression in the sea surface, colder sea

surface temperatures, local maximums in nutrients and zooplankton, domed isosurfaces, and several different currents. There is an offshore equatorward surface flow, an inshore poleward surface flow, and a poleward undercurrent. The combination of wind stress and wind-stress curl results in the appearance of the coastal upwelling signature nearshore and the offshore signature of Ekman pumping. The relative strength of the inshore and offshore features depends on the relative strengths of the wind stress and wind-stress curl and the location of the maximum curl. A combination of equatorward wind stress and negative wind-stress produces reduced coastal upwelling and offshore downwelling. On the other hand, Ekman upwelling enhances the effects of coastal upwelling. Rossby wave dynamics bring the system into steady-state equilibrium.

In general the prevailing winds along the west coast of the United States are equatorward. The CCS is located on the eastern flank of the North Pacific High. In the summer, there is a low-pressure system in the southwestern United States. Together these systems force strong equatorward winds along the coastline. The winds also undergo topographic forcing, aligning them with the coastline. Downcoast (equatorward) winds typically are strongest offshore while upcoast (poleward) winds are strongest nearshore. These patterns produce perennial positive wind-stress curl along most of the California coast. Measurements of the wind fields place the maximum wind stress (contour of zero-curl) from 100-300 km offshore and the maximum wind-stress curl approximately 5-20 km offshore. Atmospheric models of the wind field place the maximum wind stress much closer inshore, approximately 60 km offshore, and the maximum curl is typically further offshore than in the observations. Also, the magnitude of the modeled curl tends to be smaller than the measured curl.

The California Current System exhibits many key signals of coastal upwelling and Ekman pumping. The CCS has a perennial broad offshore equatorward surface flow and a poleward undercurrent. During the winter, the CCS has an inshore poleward surface flow. This flow is replaced in the spring and summer by a strong inshore equatorward surface jet. This jet develops over the entire continental shelf and eventually propagates westward into deeper waters, joining and renewing the perennial offshore equatorward flow. Offshore, the isotherms and isopycnals form domes; inshore they tilt towards the coast. During the spring and summer, the coldest sea surface temperatures are immediately adjacent to the shore. Zooplankton and nutrient abundances are found nearshore and also offshore in the region of flow reversal between the surface offshore and inshore currents.

Studies of the wind effects on the California Current show qualitatively excellent agreement between predictions and observations. The inshore and offshore currents are in approximately the predicted locations and occur at the right seasons. The isosurfaces behave as predicted, as do the sea surface temperatures and surface heights. Moreover, there is westward propagation of the shelf anomalies, akin to Rossby wave dynamics. Quantitatively the predictions and observations do not agree as well. For instance, the predicted currents are too deep, too broad, and/or too weak. However, many of these mismatches could be related to the inaccuracies of the modeled wind fields. The eddy-resolving model produced results that compared quantitatively well with observations. Overall, the studies concluded that the wind stress and the wind-stress curl control the seasonal dynamics of the California Current System. Rossby wave dynamics explain the signature westward propagation within the system. The specific spatial and temporal

details of the dynamics depend on the properties of the wind field – its cross-shore profile, the relative strength of the wind stress and wind-stress curl, and the locations of the maximum and zero wind-stress curl.

Figures

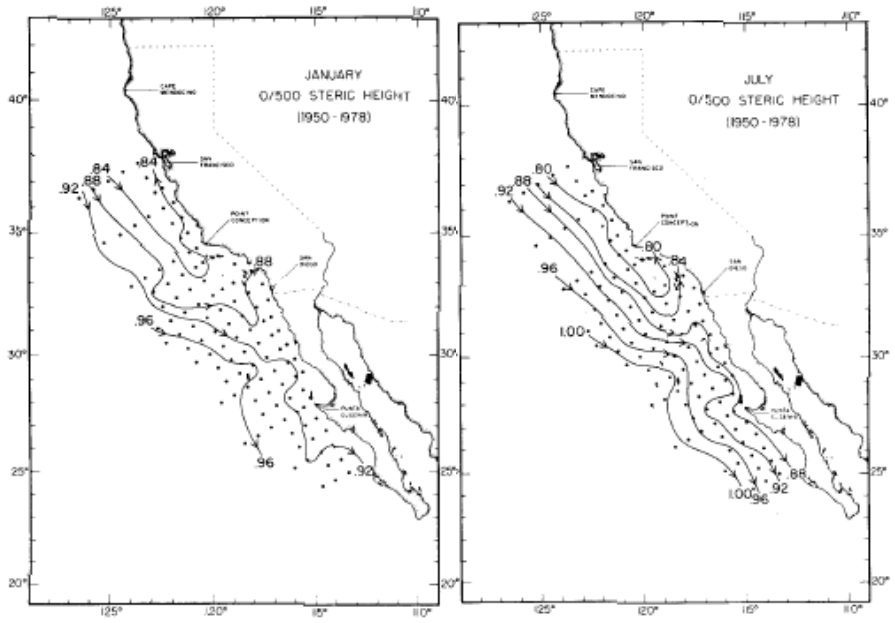

Figure 1. "January and July seasonal mean values of the steric height of the sea surface relative to 500 db. Arrows on contours indicate direction of geostrophic flow (computed from gradients of the steric height). Averages were computed over the 30-year period from 1950-80 using harmonic analysis." Chelton (1982)

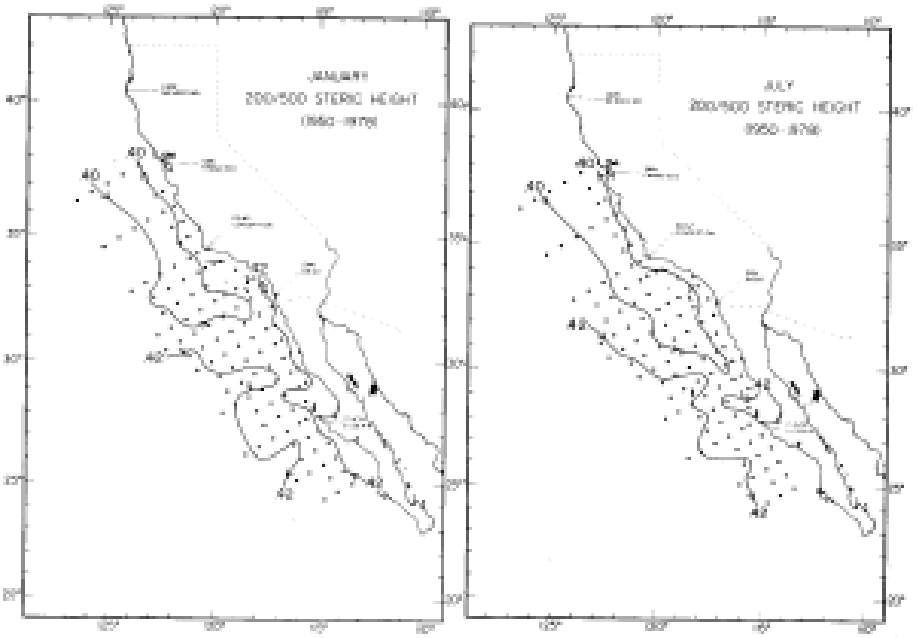

Figure 2. "Similar to Figure 1, except maps are of the steric height at 200 db relative to 500 db." Chelton (1982)

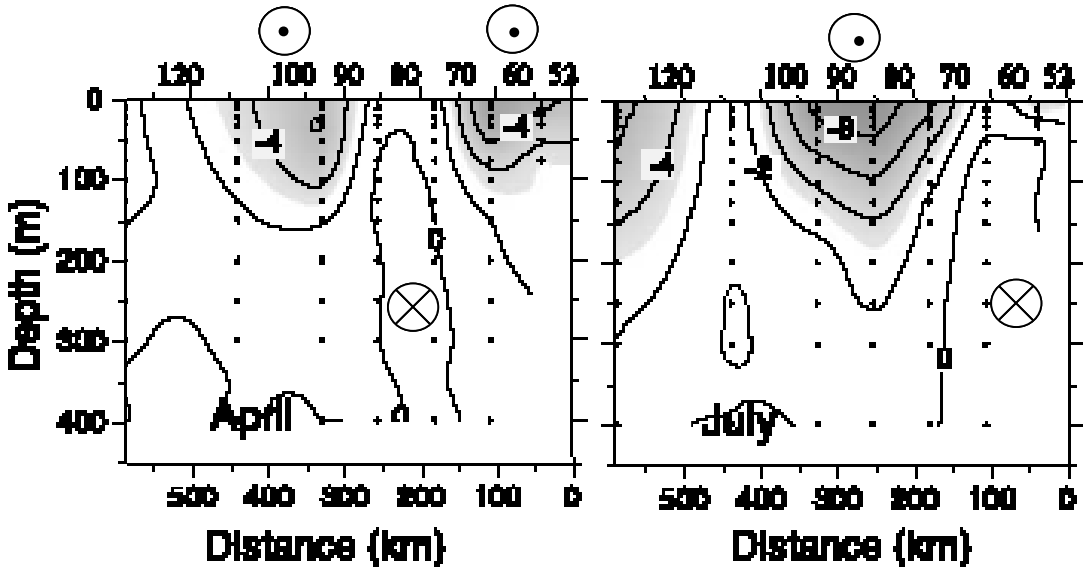

Figure 3. "Long-term mean geostrophic velocity across CalCOFI line 60 (off Pt. Reyes, 240°T) for two seasons." Lynn et al. (2003)

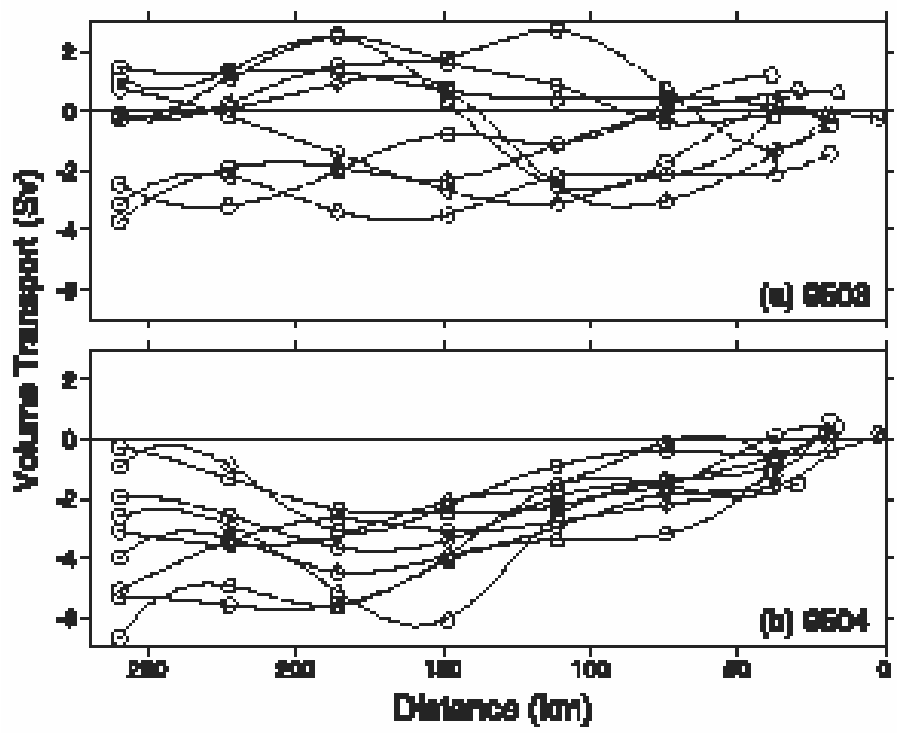

Figure 4. "Accumulated volume transport (10^6 m^3s^{-1}; relative to 1000 dbars) starting at the nearshore station pairs for the nine central lines of surveys (a) 9503 and (b) 9504." Lynn et al. (2003)

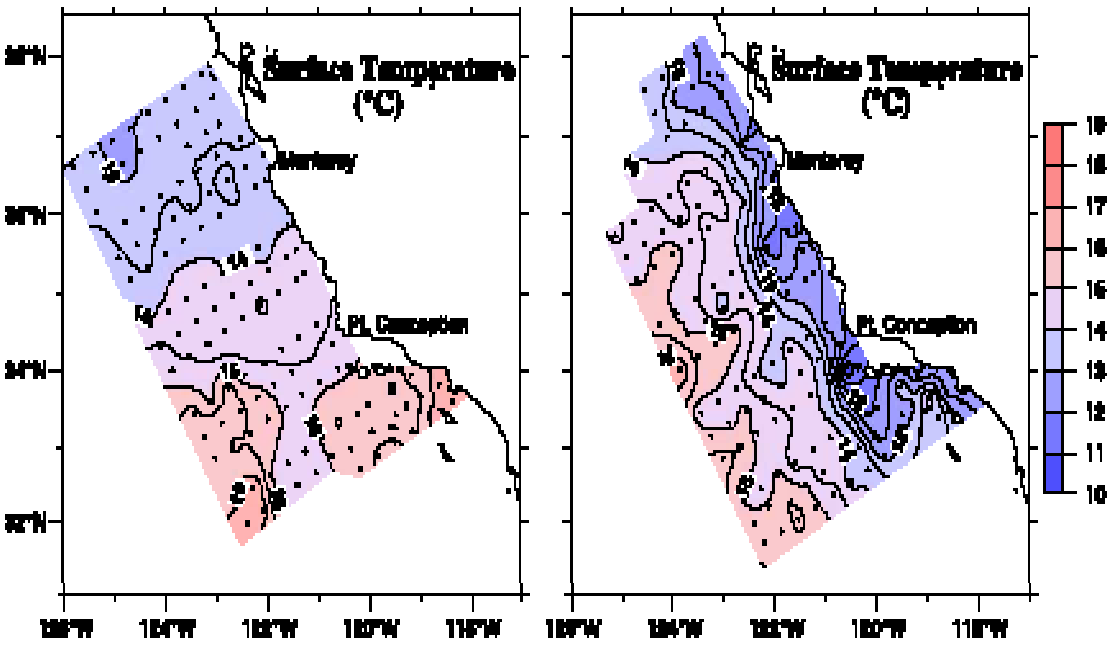

Figure 5. "Surface temperature (^{o}C)" Lynn et al. (2003)

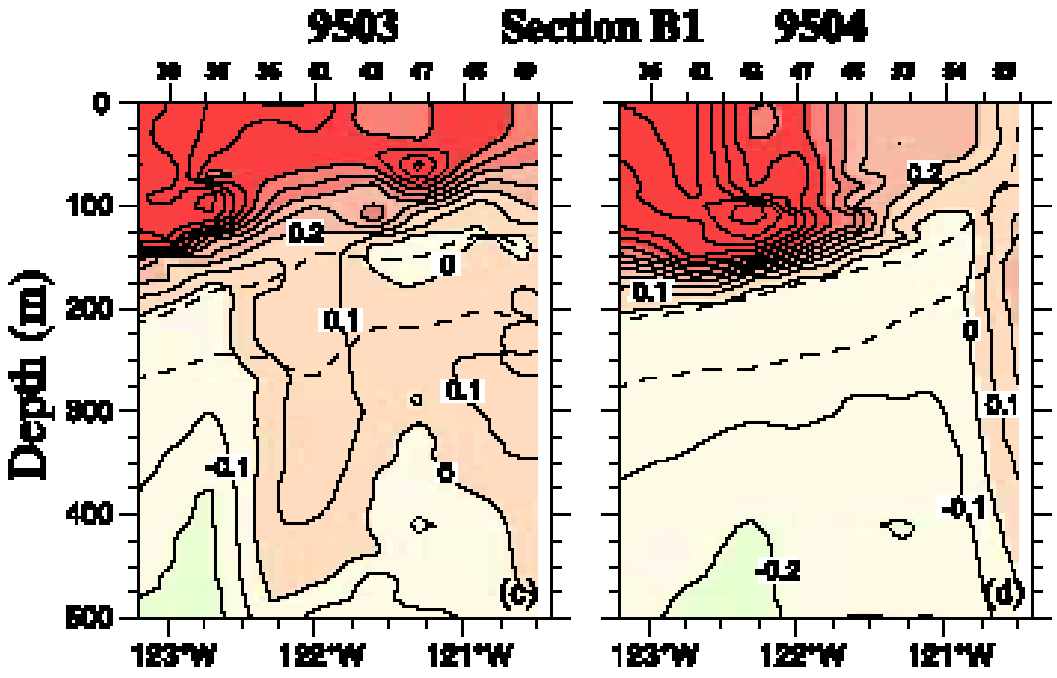

Figure 6. "Cross section of spiciness (kg m^{-3}) for surveys (left) 9503 and (right) 9504. The σ_θ=26.0 and σ_θ =26.4 kg m^{-3} isopycnal surfaces are shown with dashed lines." Lynn et al. (2003)

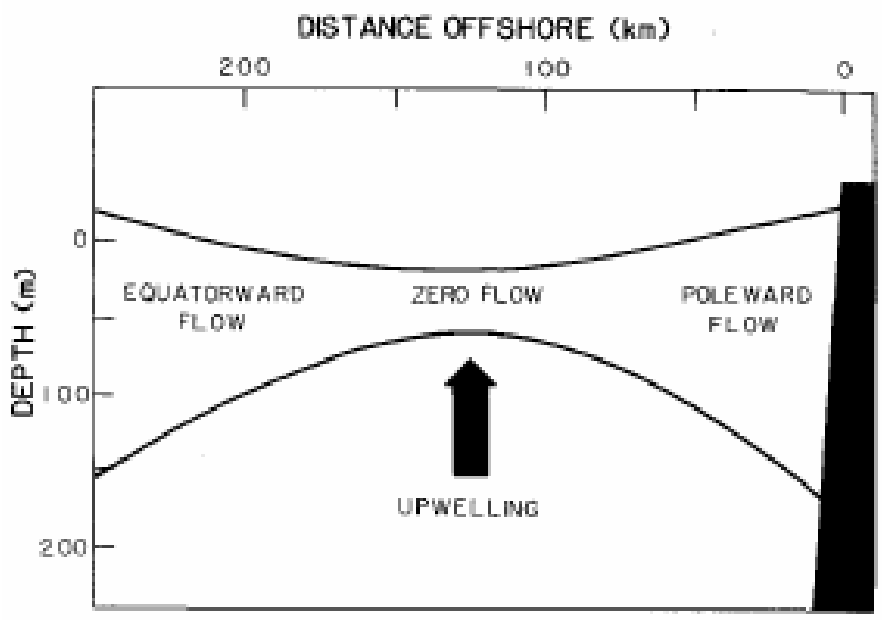

Figure 7. “Schematic diagram of two-layer system showing the sea-surface and thermocline configuration corresponding to an equatorward flow offshore and a nearshore poleward flow.” Chelton (1982)

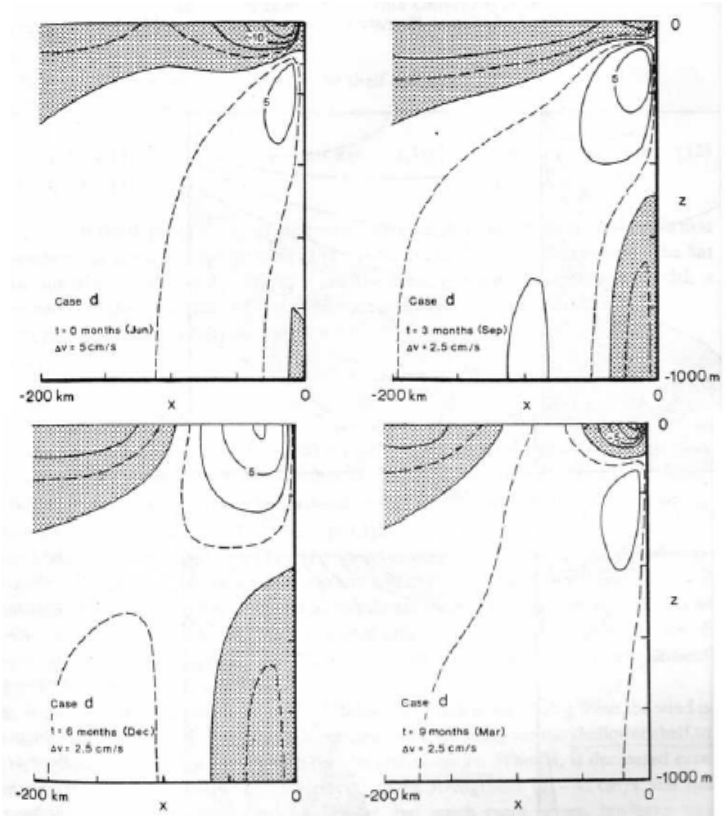

Figure 8. Solutions to the flat-bottom analytical model. "Zonal sections at 35N showing *v* at four times of the year when the wind is an idealized version of the wind field off Point Conception. Dashed contours at +/- Δ*v*/2, and regions of negative flow are shaded." McCreary et al. (1987)

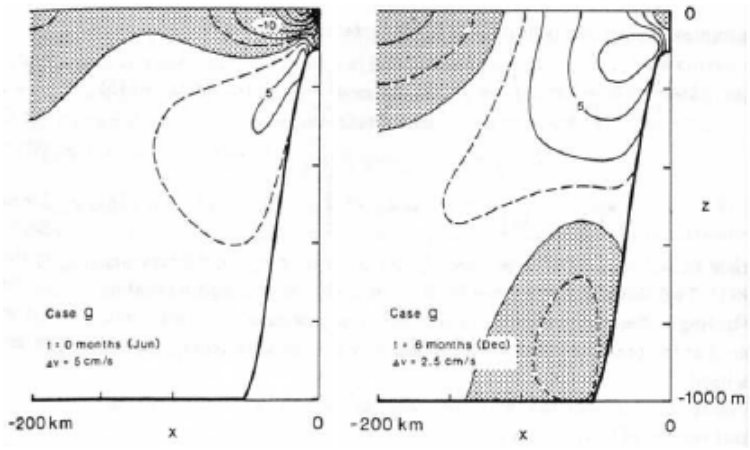

Figure 9. Solutions to the numerical model including a continental shelf. "Zonal sections at 35N showing v at two times of the year when the wind is an idealized version of the wind field off Point Conception. Dashed contours are +/- Δ*v*/2, and regions of negative flow are shaded." McCreary et al. (1987)

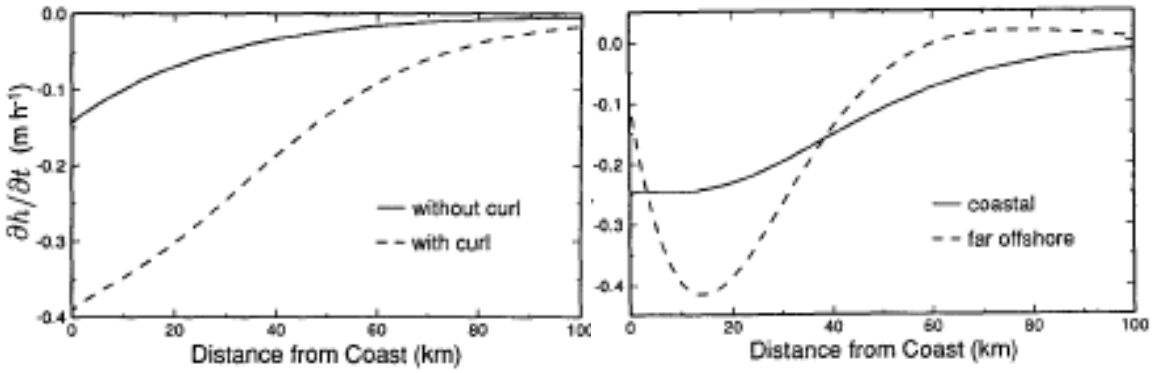

Figure 10. Analytical model steady-state solutions showing the effect of wind-stress curl on upwelling rates. Left-hand plot shows the upwelling rate for solutions forced by wind stress (solid curve) and wind stress plus wind-stress curl (dashed line). Right-hand plot shows the increase in upwelling rate due to the application of positive inshore curl (solid curve) and positive offshore curl (dashed curve). Enriquez and Friehe (1995)

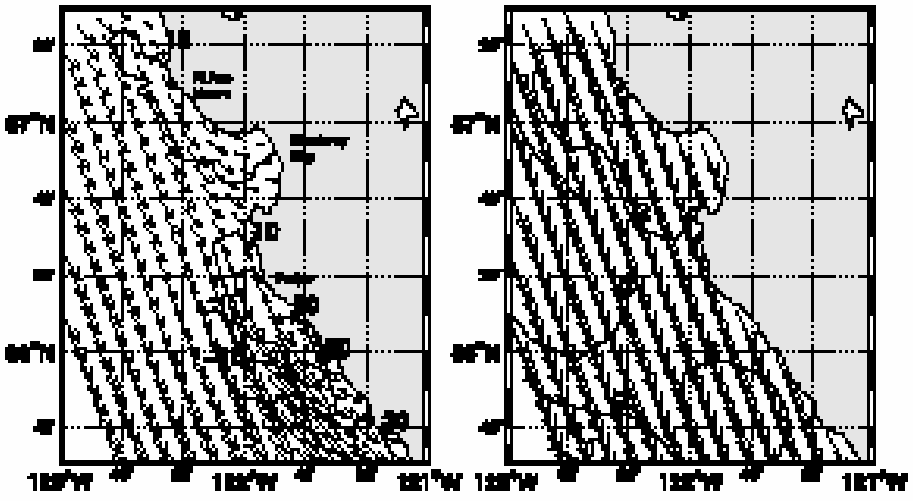

Figure 11. "Summer-mean central California wind stress (arrows; the maximal value is 0.146 Nm^{-2}) and curl (isolines, in Pa/100 km) for both BLD (left) and QCT (right)." Capet et al. (2004)

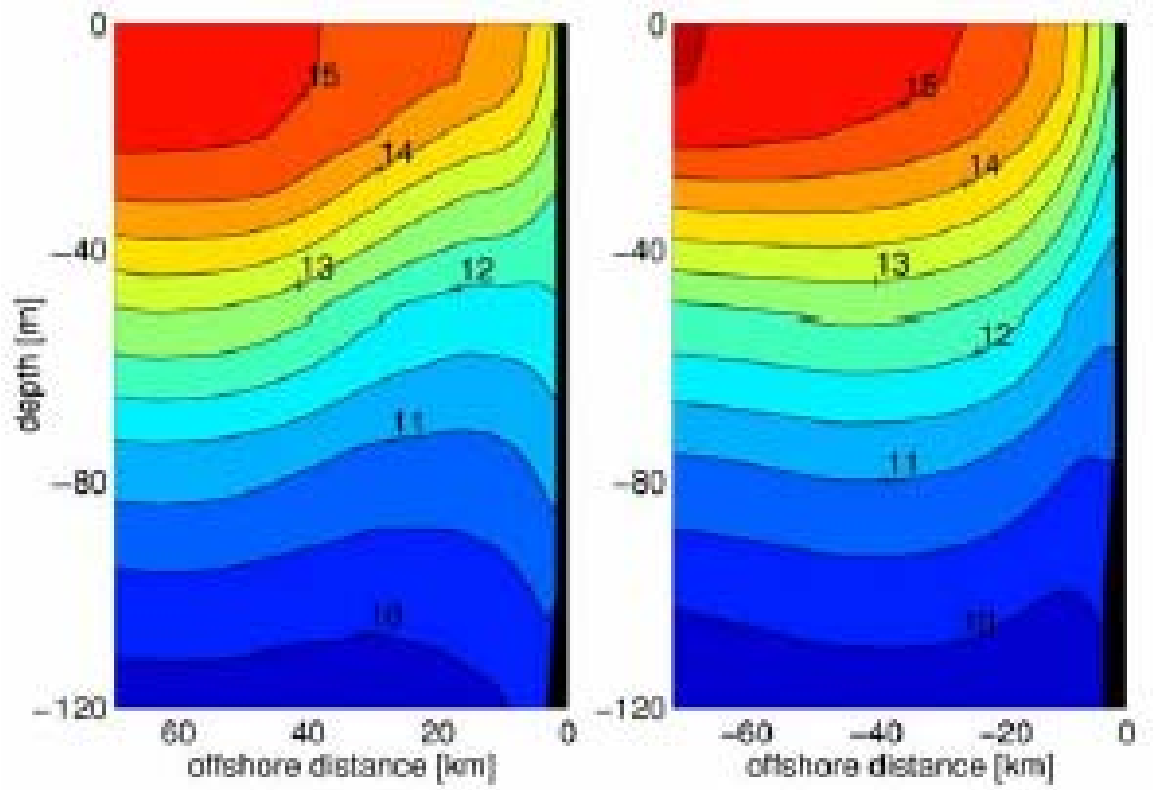

Figure 12. "Cross sections off Pt. Sur of temperature (^{o}C), averaged over the summer season and 30 km alongshore. The model is forced with either BLD (left) or QCT (right) winds." Capet et al. (2004)

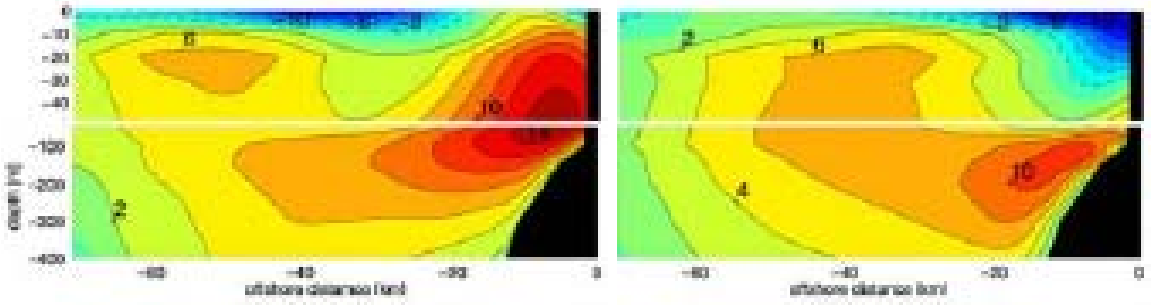

Figure 13. "Cross sections off Pt. Sur of alongshore velocity (in cm s^{-1}). The interval between 2 isolines is 2 cm s^{-1}. The model is forced with either BLD (left) or QCT (right) winds." Capet et al. (2004)

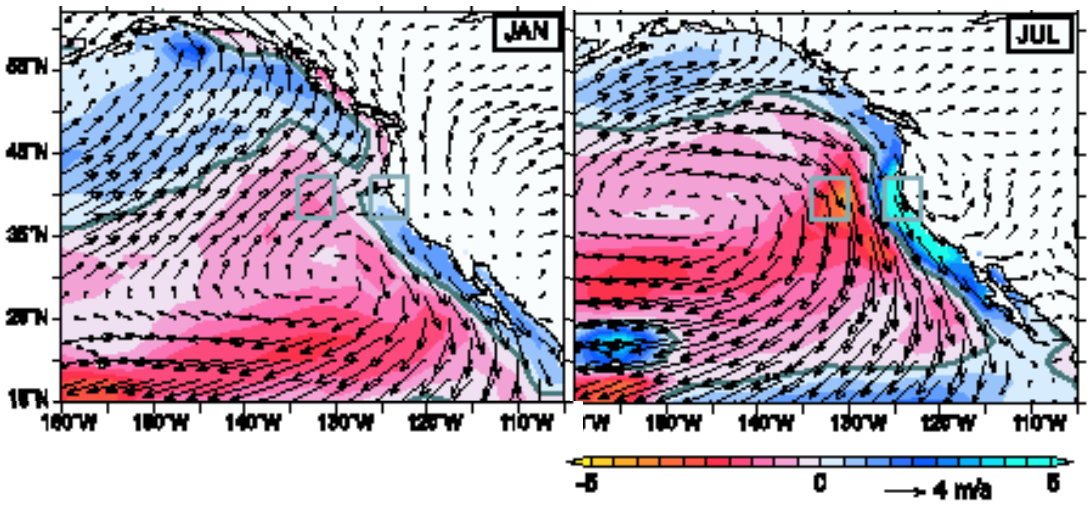

Figure 14. "Climatological surface winds (vectors) and wind stress curl (color shading; N m^{-3}) for January (left) and July (right). We use blue (red) for positive (negative) WSC." Murphree et al. (2003)

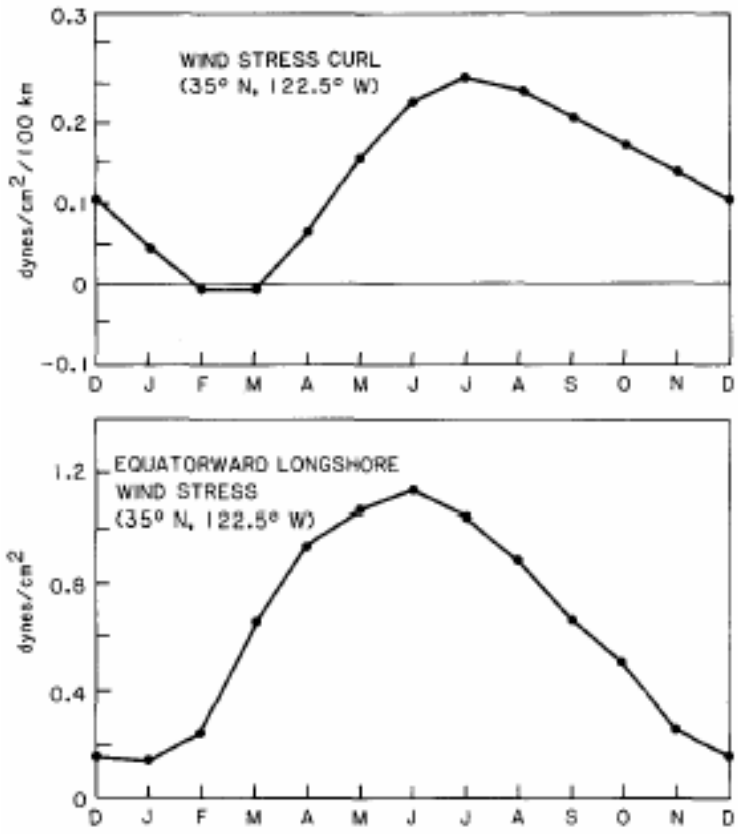

Figure 15. "Seasonal variation of the wind stress curl at 35N, 122.5W (upper panel). Seasonal variation of the equatorward longshore wind stress at 35N, 122.5W (lower panel)." Chelton (1982)

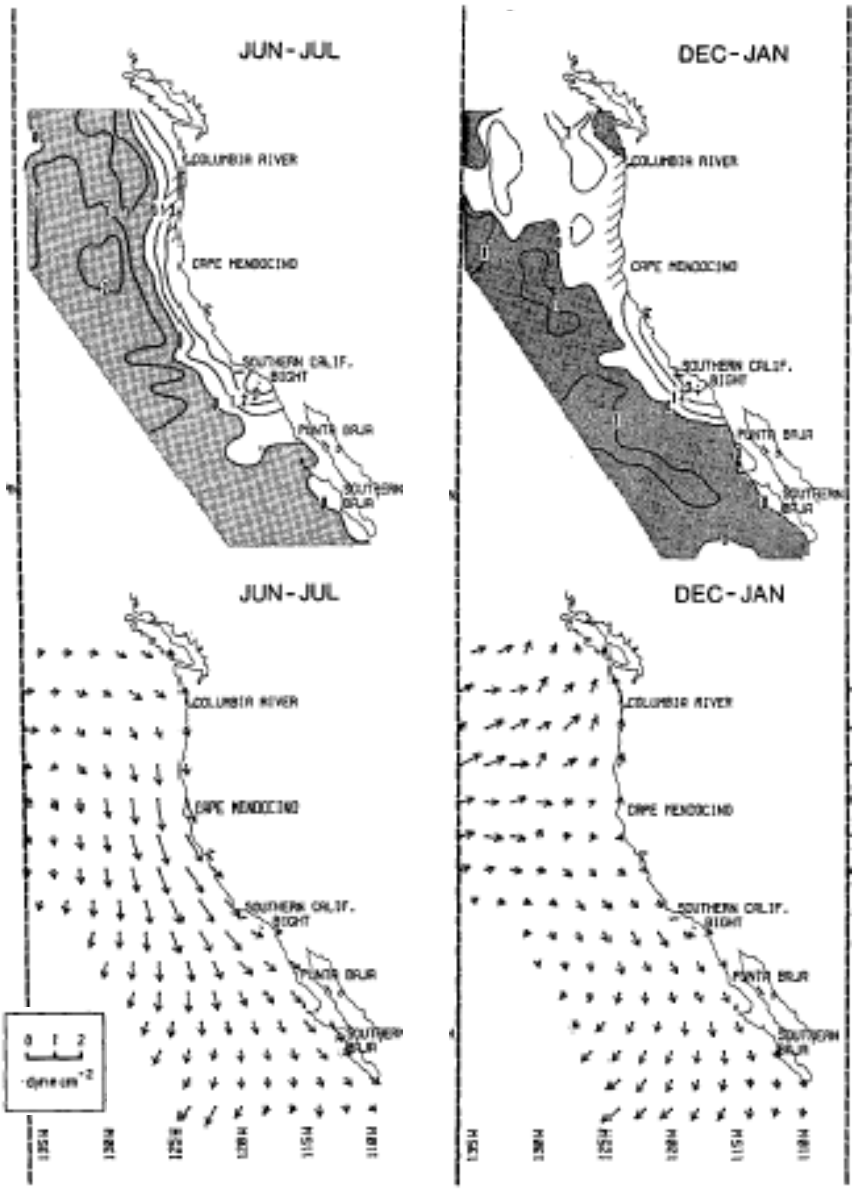

Figure 16. "Wind-stress curl (10^{-8} dyn cm^{-3}) and surface wind stress (dyn cm^{-2}) distributions. Contour interval is 1 x 10^{-8} dyn cm^{-3} and regions of anticyclonic curl are shaded. Wind-stress vectors are plotted at alternate latitude and longitude intersections, and symbols are scaled according to the key on the chart." Bakun and Nelson (1991)

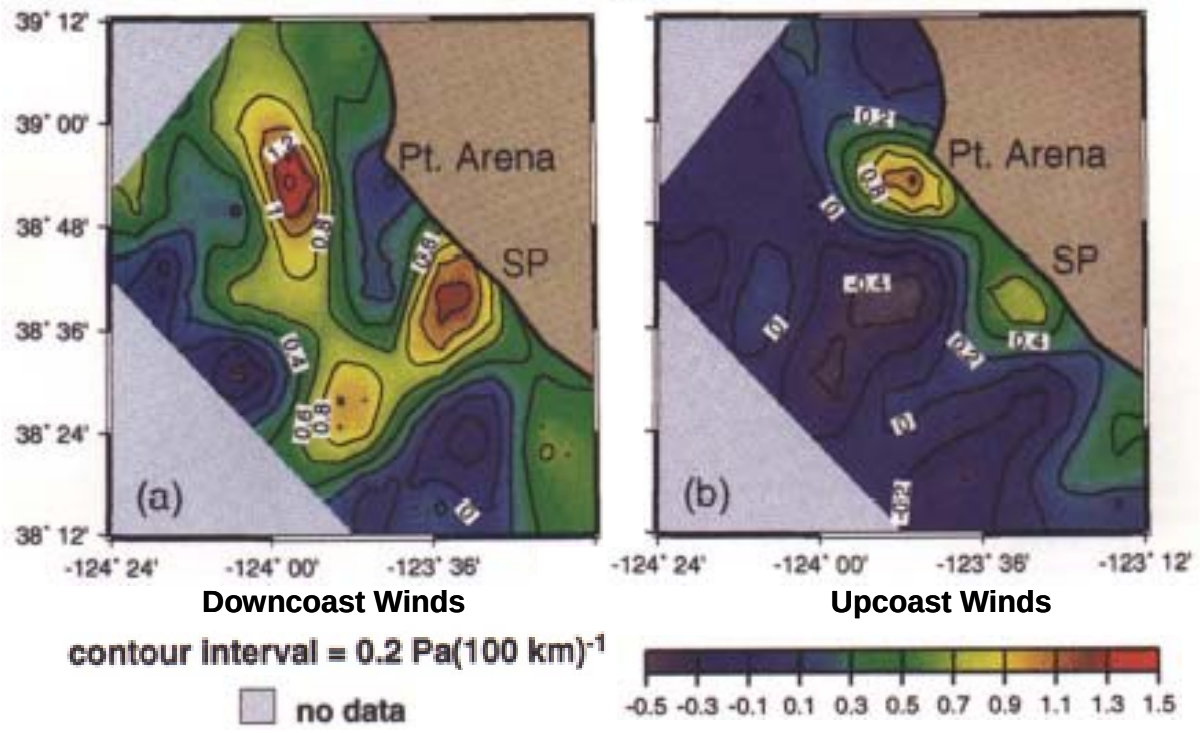

Figure 17. "Curl of wind stress [in Pa (100 km)$^{-1}$] for (a) downcoast winds and (b) upcoast winds. Stewarts Point in indicated as SP." Enriquez and Friehe (1995)

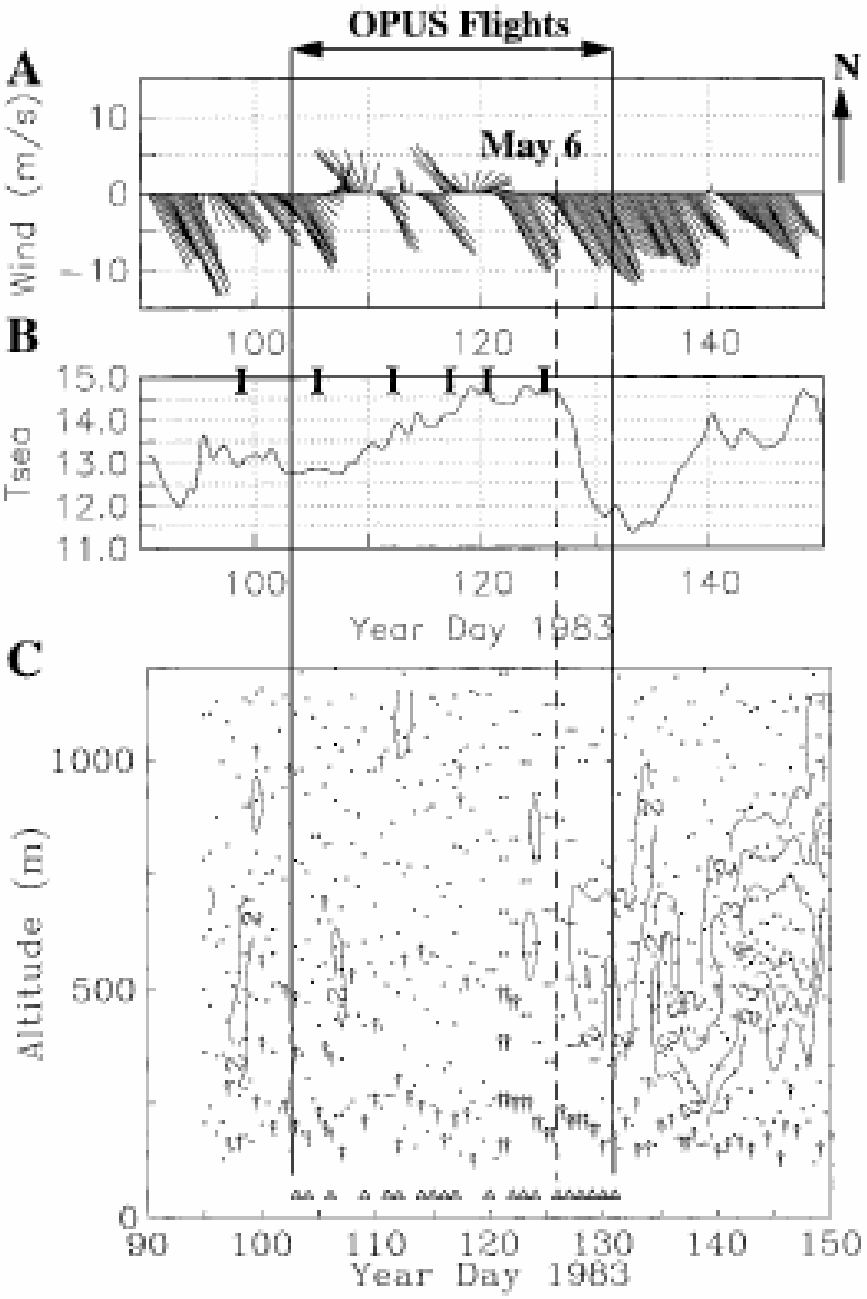

Figure 18. "Time series of (a) winds at NOAA environmental buoy 46023, (b) sea surface temperature (SST) at the buoy, and (c) buoyancy frequency (N) in the lower atmosphere at Vandenberg AFB. The units in (c) are 10^{-2} s^{-1} and, for clarity, only contours > 1 x 10^{-2} s^{-1} are shown. Note that all CTD surveys [vertical bars in (b)] were done prior to the persistent upwelling-favorable winds. The times of the 20 aircraft flights are indicated at the bottom of (c) as triangles. Dots indicate the location of measurements. Unstable vertical density gradients are indicated by a vertical arrow." Münchow (2000)

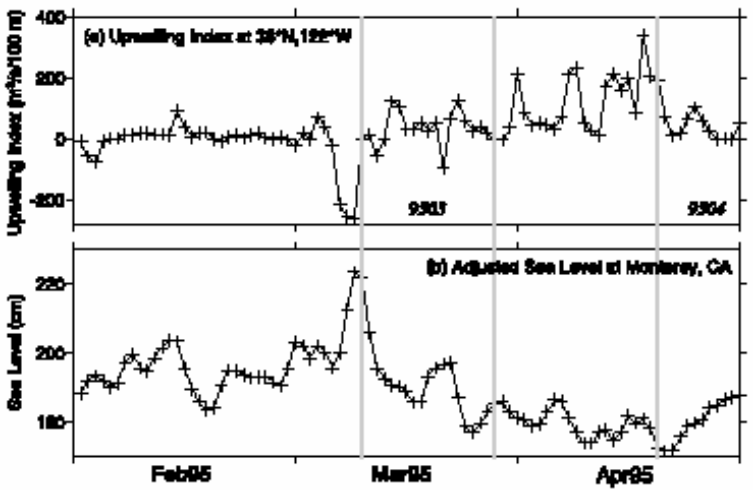

Figure 19. "Time series (February – April 1995) of (a) daily upwelling index (m^3 s^{-1} per 100 m coastline) from 36°N, 122°W and (b) daily adjusted sea level (cm) from Monterey, California. Periods of surveys are marked with gray lines." Lynn et al. (2003)

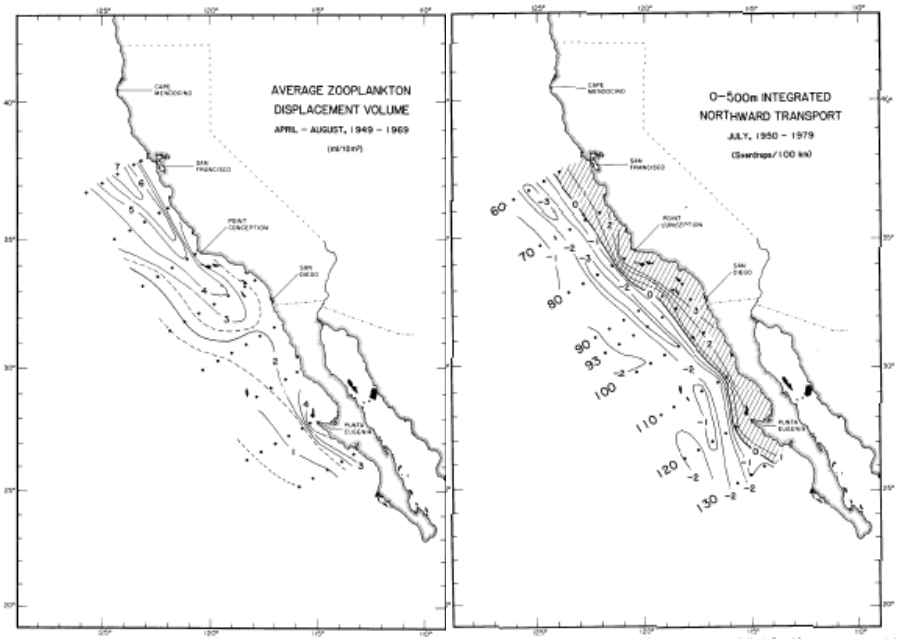

Figure 20. (Left) "Spring-summer distribution of zooplankton displacement volume in the California Current. April-August long-term (1949-69) averages were computed over 'pooled areas' measuring 200 km in the longshore direction and 65 km in the cross-shore direction. The dots represent the centers of the pooled areas. This spatial and temporal averaging removes the small-scale patchiness inherent in the zooplankton samples." (Right) "Seasonal average longshore integrated geostrophic transport in the upper 500 m in the California Current for July. Transport was calculated from geostrophic velocities relative to a reference level of 500 db (dots show location of stations used to draw contours, and the CalCOFI line numbers are labeled). Shaded region represents poleward transport." Chelton (1982)

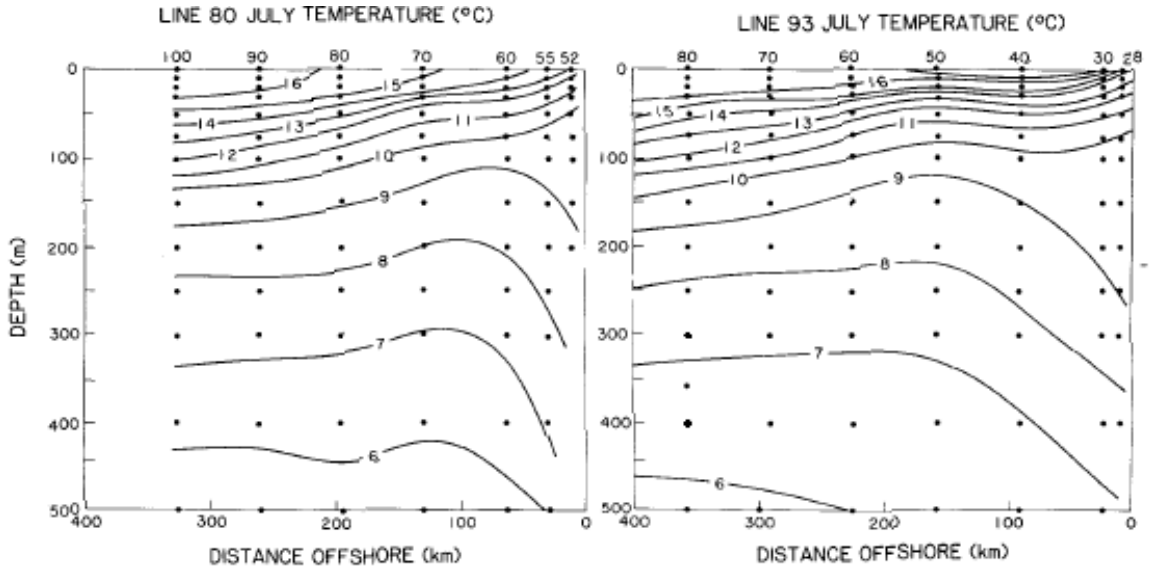

Figure 21. "Average July temperature sections along CalCOFI lines 80 and 93 computed by a harmonic method over the 30-year period 1950-79. CalCOFI station numbers are shown along the top of each plot." Chelton (1982)

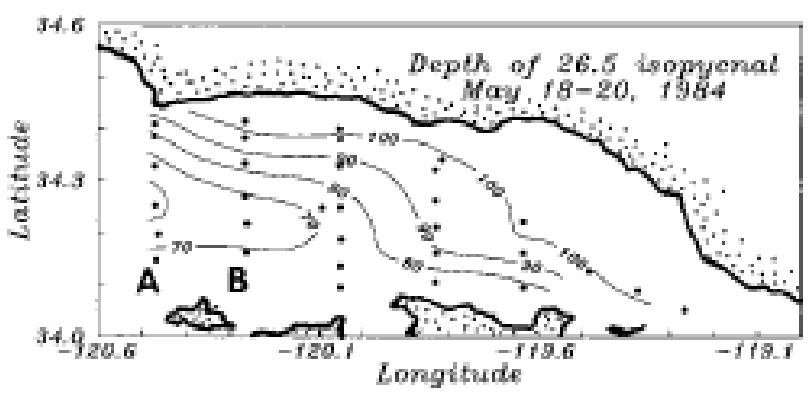

Figure 22. "Depth of the 26.5 σ_t density surface. Labels 'A' and 'B' refer to the two density sections shown in Fig." 20. "Filled circles indicate the location of CTD stations." Münchow (2000)

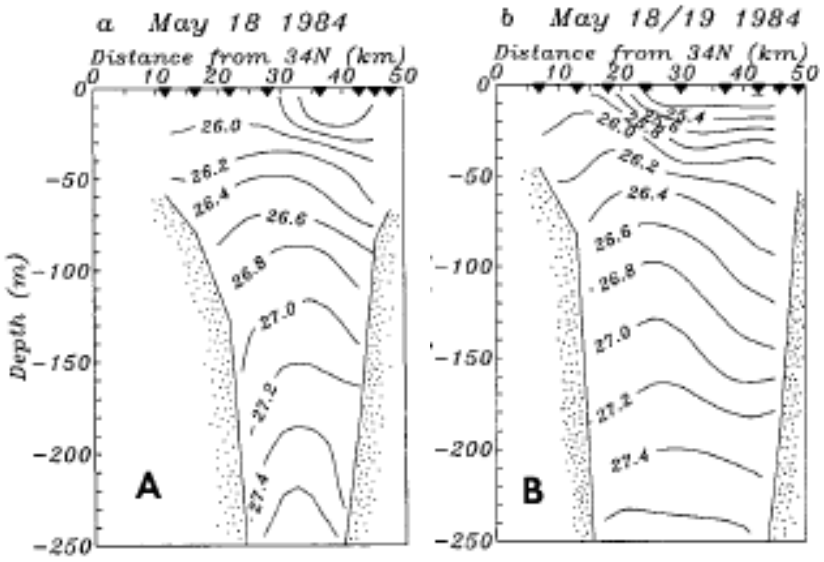

Figure 23. "Two density sections across the western Santa Barbara Channel. The locations for transects A and B, as shown in Fig." 19, "are labeled 'A' and 'B,' respectively." Münchow (2000)

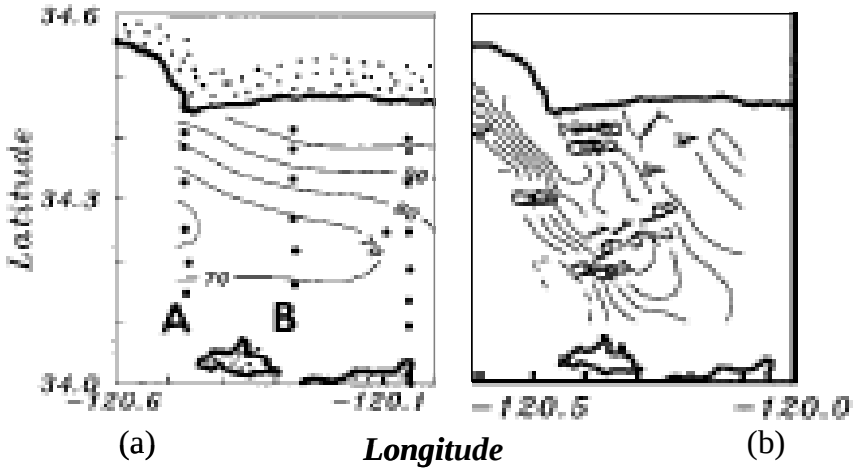

Figure 24. (a) Depth of the 26.5 density surface near Point Conception on May 19, 1984. (b) Vertical Ekman pumping velocities on May 8, 1983, positive velocities are upward. From Münchow (2000)

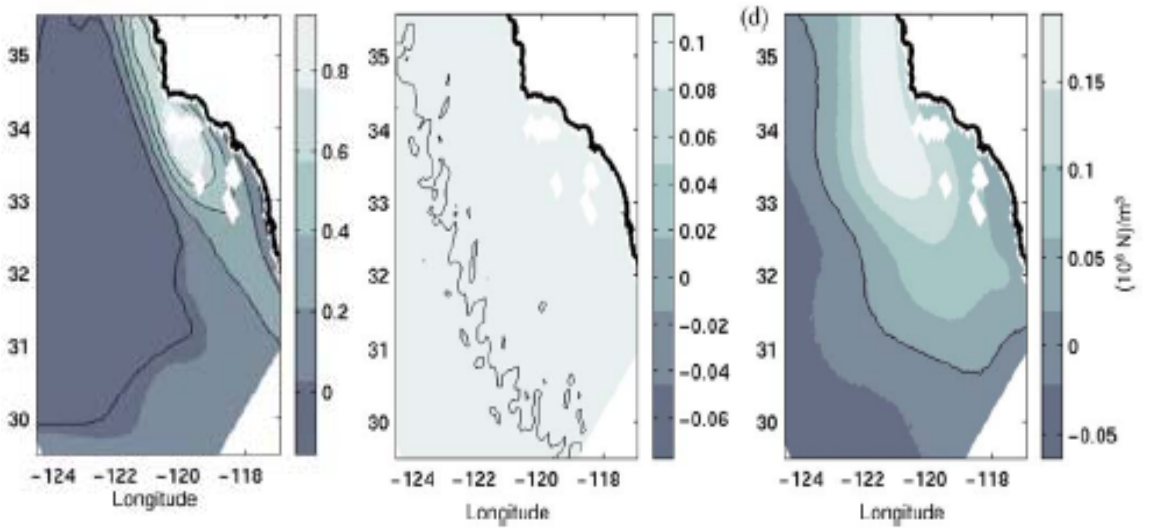

Figure 25. "Mean wind stress curl of (left to right) RSM winds, COADS 2 x 2, and NCEP Pacific Ocean Analysis. The color bars are different on each panel in order to better show the contours." Di Lorenzo (2003)

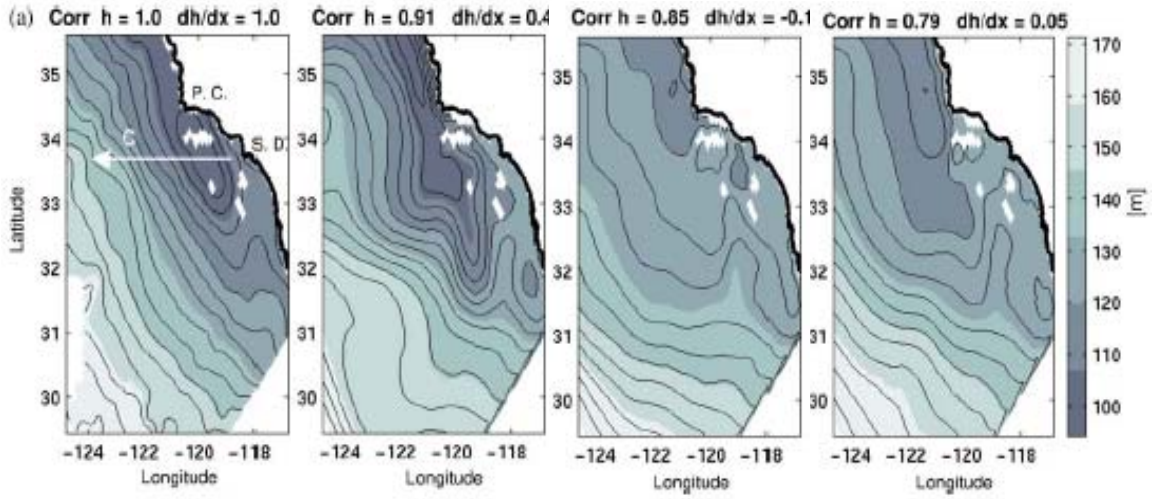

Figure 26. "Mean depth *h* of the 26.5 isopycnal (a) from CalCOFI observations compared to the one obtained by integrating the model with the (b) RSM winds, (c) COADS 2 x 2, and (d) NCEP Pacific Ocean Analysis. On the top correlation coefficient (against the observation in a) for the depth *h* and zonal gradient d*h*/dx." The transect "C" is referenced in the text and in Figure 27. Di Lorenzo (2003)

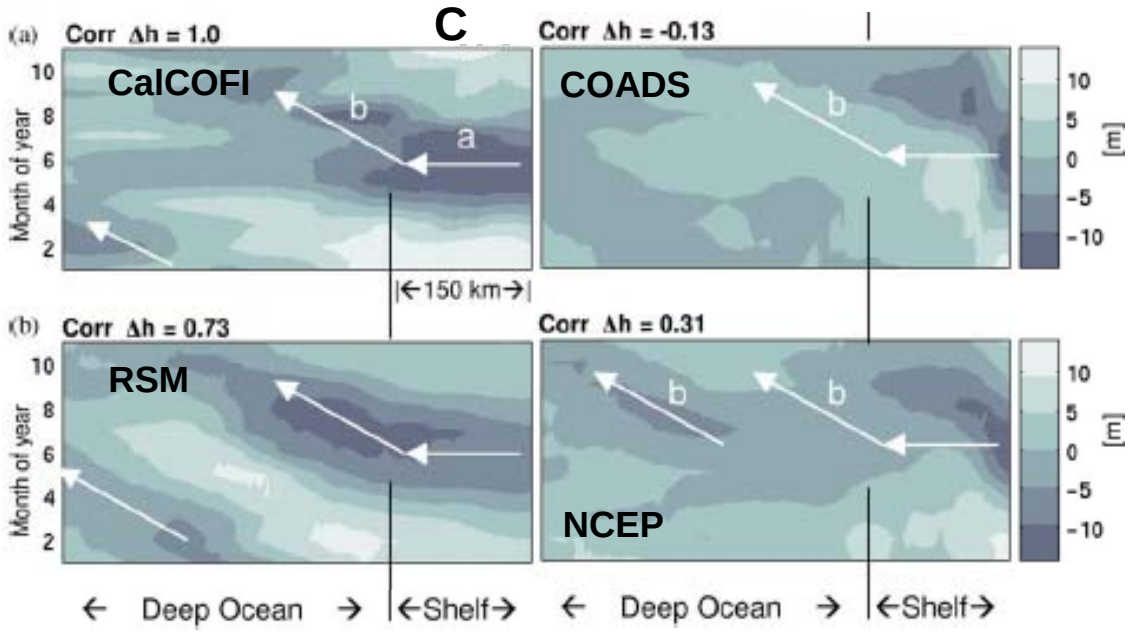

Figure 27. "Westward transect C (x-axis) of the mean 26.5 isopycnal depth anomaly (Δh) as a function of month of the year (y-axis): (a) CalCOFI observations, (b) case RSM winds, (c) case COADS 2 x 2, and (d) case NCEP Pacific Ocean Analysis. Correlation coefficients with (a) are plotted in the top left corner of each panel." Di Lorenzo (2003)

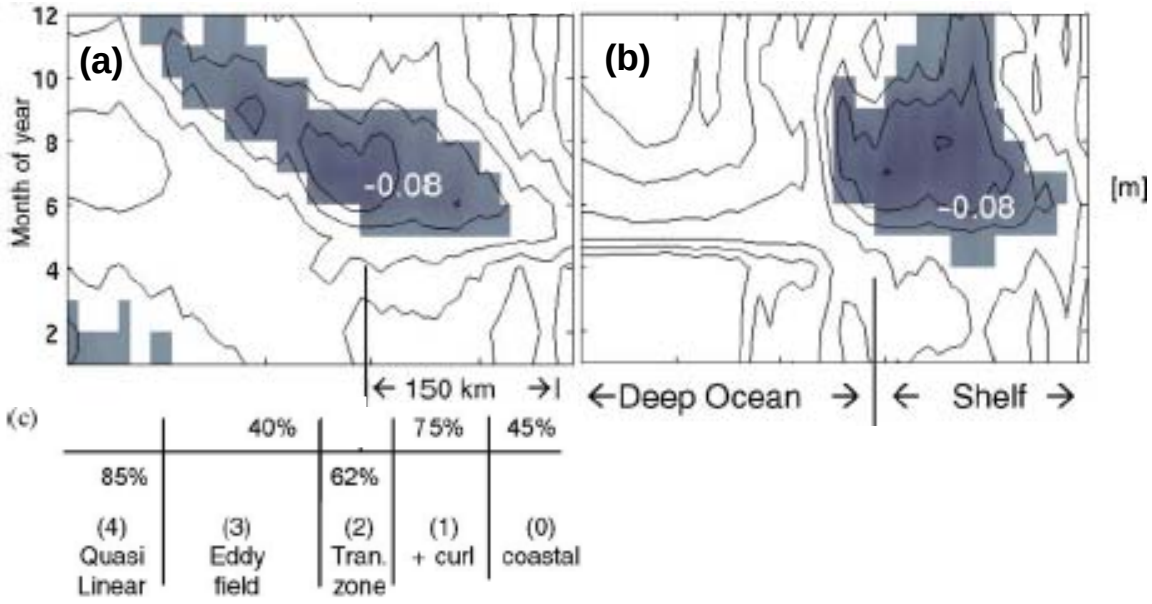

Figure 28. "Westward transect C (x-axis) of SSH anomalies (m) from the linearized model. Dark area is negative and increases towards the white (CI=0.03). Integrations with (a) $\beta \neq 0$ and with (b) $\beta = 0$. (c) Fraction of variance explained by the linearized model when compared to the non-linear as a function of cross-shore location. The variable used for the comparison is the depth anomaly of the density surface 26.5." Di Lorenzo (2003)

References

Apel, J. R., 1987. “Principles of Ocean Physics”. Academic Press, London.

Bakun, A., & Nelson, C. S., 1991. The seasonal cycle of wind-stress curl in subtropical eastern boundary current regions. *Journal of Physical Oceanography, 21*(12), 1815-1834.

Capet, X. J., Marchesiello, P., & McWilliams, J. C., 2004. Upwelling response to coastal wind profiles. *Geophysical Research Letters, 31*(13).

Chelton, D. B., 1982. Large-scale response of the California Current to forcing by the wind stress curl. *California Cooperative Oceanic Fisheries Investigations Reports, Vol. XXIII*, 130-148.

Di Lorenzo, E., 2003. Seasonal dynamics of the surface circulation in the Southern California Current System. *Deep-Sea Research, Part II, 50*, 2371-2388.

Enriquez, A. G., & Friehe, C. A., 1995. Effects of wind stress and wind stress curl variability on coastal upwelling. *Journal of Physical Oceanography, 25*(7), 1651-1671.

Gill, A. E., 1982. “Atmosphere-Ocean Dynamics”. Academic Press, San Diego and London.

Lynn, R. J., Bograd, S. J., 2002. Dynamic Evolution of the 1997-1999 El Niño-La Niña cycle in the southern California Current System. *Progress in Oceanography, 54*, 59-75.

Lynn, R. J., Bograd, S. J., Chereskin, T. K., & Huyer, A., 2003. Seasonal renewal of the California Current: The spring transition off California. *Journal of Geophysical Research, 108*(C8), 35-1 – 35-11.

Marchesiello, P., McWilliams, J. C., & Shchepetkin, A., 2003. Equilibrium structure and dynamics of the California Current System. *Journal of Physical Oceanography, 33*(4), 753-783.

McCreary, J. P., Jr, Kundu, P. K., & Chao, S., 1987. On the dynamics of the California Current System. *Journal of Marine Research, 45*(1), 1-32.

Münchow, A., 2000. Wind stress curl forcing of the coastal ocean near Point Conception, California. *Journal of Physical Oceanography, 30*(6), 1265-1280.

Murphree, T., Green-Jessen, P., Schwing, F. B., & Bograd, S. J., 2003. The seasonal cycle of wind stress curl and its relationship to subsurface ocean temperature in the Northeast Pacific. *Geophysical Research Letters, 30*(9).

Tomczak, M., Godfrey, J. S., 2003. "Regional Oceanography: An Introduction," 2nd ed. Daya Publishing House, Delhi.